arXiv:cond-mat/0504608v2 [cond-mat.other] 13 May 2006

Wavelet versus Detrended Fluctuation Analysis of multifractal structures

Paweł Oświęcimka,[1] Jarosław Kwapień,[1] and Stanisław Drożdż[1,2]

[1] *Institute of Nuclear Physics, Polish Academy of Sciences, Kraków, Poland*
[2] *Institute of Physics, University of Rzeszów, Rzeszów, Poland*

(Dated: February 9, 2022)

We perform a comparative study of applicability of the Multifractal Detrended Fluctuation Analysis (MFDFA) and the Wavelet Transform Modulus Maxima (WTMM) method in proper detecting of mono- and multifractal character of data. We quantify the performance of both methods by using different sorts of artificial signals generated according to a few well-known exactly soluble mathematical models: monofractal fractional Brownian motion, bifractal Lévy flights, and different sorts of multifractal binomial cascades. Our results show that in majority of situations in which one does not know a priori the fractal properties of a process, choosing MFDFA should be recommended. In particular, WTMM gives biased outcomes for the fractional Brownian motion with different values of Hurst exponent, indicating spurious multifractality. In some cases WTMM can also give different results if one applies different wavelets. We do not exclude using WTMM in real data analysis, but it occurs that while one may apply MFDFA in a more automatic fashion, WTMM has to be applied with care. In the second part of our work, we perform an analogous analysis on empirical data coming from the American and from the German stock market. For this data both methods detect rich multifractality in terms of broad $f(\alpha)$, but MFDFA suggests that this multifractality is poorer than in the case of WTMM.

I. INTRODUCTION

It is well-known that the self-similarity of fractal structures can be described by the so-called Hölder exponents or the local Hurst exponents α. If the fractal is homogenous (monofractal) then it can be associated with only one Hölder exponent, while in the case of a multifractal, different parts of the structure are characterized by different values of α, leading to the existence of the whole spectrum $f(\alpha)$. In contrast to model fractals with a precise scaling, many fractals, both the mathematical and the natural, reveal only a statistical scaling and this in particular refers to the so called fractal signals. An exemplary temporal process with a trivial monofractal scaling is the fractional Gaussian noise; this process has only one α equal to 0.5 for the uncorrelated motion and $\alpha \neq 0.5$ if any linear correlations exist in the signal. On the other hand, a process with either non-Gaussian fluctuations or with nonlinear temporal correlations can be multifractal, and two or more values of α or even a continuous spectrum $f(\alpha)$ can be needed to characterize structure of such a process.

In recent years much effort has been devoted to reliable identification of the multifractality in real data coming from such various fields like e.g. DNA sequences [1, 2, 3], physiology of human heart [4, 5], neuron spiking [6], atmospheric science and climatology [7, 8, 9, 10], financial markets [11, 12, 13, 14, 15, 16, 17, 18, 19, 20], geophysics [21] and many more. This is, however, a difficult task mainly due to the fact that experimental data related to physiology, economy or climate is highly nonstationary and, additionally, the available data samples are usually rather small. One thus requires to apply methods which are insensitive to nonstationarities like trends and heteroskedasticity. In principle there are two competitive methods of detection of the multifractality which are commonly used in this context; both supposed to eliminate trends and concentrate on the analysis of fluctuations. Multifractal Detrended Fluctuation Analysis (MFDFA) [1, 22, 23] is based on the identification of scaling of the qth-order moments that power-law depend on the signal length and is a generalization of the standard DFA using only the second moment $q = 2$. The other method, Wavelet Transform Modulus Maxima (WTMM) [24, 25, 26], consists in detection of scaling of the maxima lines of the continuous wavelet transform on different scales in the time-scale plane. This procedure is advocated as especially suitable for analyzing the nonstationary time series [27].

We therefore we shall test and compare the applicability of those two methods to the data coming from either a few mathematical fractal models or empirical data collected from the stock market. In this work we represent a point of view of a practitioner who wants to choose a better tool for his analyses without entering subtle theoretical considerations. A deeper analytical research, although important and desired in general, remains beyond the scope of this work.

That data from various markets like the stock market, the foreign currency market and the commodity one are of multifractal nature, it is well-known from a numerous recent studies [11, 12, 13, 14, 15, 16, 17, 18, 19, 20], that were carried out with the help of both methods. A few years ago the Multifractal Model of Asset Returns was developed [35, 36] in order to explain the origin of this multifractality. This model and its later modifications [37, 38, 39, 40] use the multiplicative cascades which generate signals that are inherently multifractal and that are able to mimic some key properties of financial data. The rationale behind the introduction of such a model was the observed correspondence between financial market evolution and fluid turbulence [41]. From

the other point of view, the existence of the so-called financial stylized facts (fat tails of the fluctuation distributions and long-lasting nonlinear correlations in the signals) [42, 43, 44, 45, 46] can also be considered a source of the multifractal dynamics [18, 19, 20].

Our paper is organized as follows: In Section 2, we briefly sketch the foundations of the MFDFA and WTMM methods. We apply them to a few types of model data like Brownian motion, Lévy process and binomial multiplicative cascades in Section 3. In Section 4 we illustrate the performance of both methods in a context of real financial signals and, finally, we arrive at the concluding remarks in Section 5.

II. DESCRIPTION OF METHODS

A. Multifractal Detrended Fluctuation Analysis

The Detrended Fluctuation Analysis [1] has recently become a commonly used tool in analyses of scaling properties of monofractal signals and in identifying correlations present in noisy nonstationary time series [22]. The multifractal generalization of this procedure (MFDFA(l)) [22] can be briefly sketched as follows. First, for a given time series $x(i),\ i = 1, ..., N$ on a compact support, one calculates the integrated signal profile $Y(j)$

$$Y(j) = \sum_{i=1}^{j} (x(i) - < x >),\ j = 1, ..., N \qquad (1)$$

where $< ... >$ denotes averaging over the time series, and then one divides it into M_n segments of length n ($n < N$) starting from both the beginning and the end of the time series (i.e. $2M_n$ such segments total). Each segment ν has its own local trend that can be approximated by fitting an lth order polynomial $P_\nu^{(l)}$ and subtracted from the data; next, the variances for all the segments ν and all segment lengths n have to be evaluated

$$F^2(\nu, n) = \frac{1}{n} \sum_{j=1}^{n} \{Y[(\nu - 1)n + j] - P_\nu^{(l)}(j)\}^2. \qquad (2)$$

Finally, $F^2(\nu, n)$ is averaged over ν's and the qth order fluctuation function is calculated for all possible segment lengths n:

$$F_q(n) = \left\{ \frac{1}{2M_n} \sum_{\nu=1}^{2M_n} [F^2(\nu, n)]^{q/2} \right\}^{1/q}, \quad q \in \mathbf{R}. \qquad (3)$$

The key property of $F_q(n)$ is that for a signal with fractal properties, it reveals power-law scaling within a significant range of n

$$F_q(n) \sim n^{h(q)}. \qquad (4)$$

The result of the MFDFA(l) procedure is the family of exponents $h(q)$ (called the generalized Hurst exponents) which, for an actual multifractal signal, form a decreasing function of q, while for a monofractal $h(q) = const$. The singularity spectrum of the Hölder exponents $f(\alpha)$ can easily be obtained from the generalized Hurst exponents by the following relations [47]

$$\alpha = h(q) + qh'(q) \qquad f(\alpha) = q[\alpha - h(q)] + 1. \qquad (5)$$

α characterizes the strength of singularities and $f(\alpha)$ can be considered the fractal dimension of a subset of the time series with singularities of strength equal to α.

B. Wavelet Transform Modulus Maxima method

The alternative Wavelet Transform Modulus Maxima method is a technique based on the wavelet transform [24, 25, 26]

$$T_\psi(n, s') = \frac{1}{s'} \sum_{i=1}^{N} \psi(\frac{i - n}{s'}) x(i) \qquad (6)$$

where ψ is a wavelet kernel shifted by n and s' is scale. The wavelet method can serve as a tool for decomposing the signal in time-scale plane; the resulting wavelet spectrum $T_\psi(n, s')$ can reveal a hierarchical structure of singularities (see Figure 1). As a criterion for the choice of the mother wavelet ψ, a good localization in space and in frequency domains is recommended. The family of wavelets which is used most frequently in this case is the mth derivative of a Gaussian

$$\psi^{(m)}(x) = \frac{d^m}{dx^m}(e^{-x^2/2}), \qquad (7)$$

because it removes the signal trends that can be approximated by polynomials up to $(m - 1)$th order [22].

In the presence of a singularity in data one observes the power law behaviour of the coefficients T_ψ

$$T_\psi(n_0, s') \sim s'^{\,\alpha(n_0)}. \qquad (8)$$

This relation, however, is not stable in the case of densely packed singularities; it is thus much better if one identifies the local maxima of T_ψ and then calculates the partition function from moduli of the maxima

$$Z(q, s') = \sum_{l \in L(s')} |T_\psi(n_l(s'), s')|^q, \qquad (9)$$

where $L(s')$ denotes the set of all maxima for scale s' and $n_l(s')$ stands for the position of a particular maximum. In order to preserve the monotonicity of $Z(q, s')$ on s', one has to impose an additional supremum condition

$$Z(q, s') = \sum_{l \in L(s')} (\sup_{s'' \le s'} |T_\psi(n_l(s''), s'')|)^q. \qquad (10)$$

For a signal with a fractal structure, we expect that $Z(q,s') \sim {s'}^{\tau(q)}$. The singularity spectrum $f(\alpha)$ can now be obtained according to the following formulas [47]

$$\alpha = \tau'(q) \quad \text{and} \quad f(\alpha) = q\alpha - \tau(q). \tag{11}$$

Additionally, there is a relation between $\tau(q)$ and the generalized Hurst exponents

$$\tau(q) = qh(q) - 1. \tag{12}$$

Linear behaviour of $\tau(q)$ indicates monofractality whereas nonlinear one suggests that a signal is multifractal. An example illustrating the WTMM procedure is shown in Figure 1 for the devil's staircase obtained by integrating the Cantor measure. It should be explained that we calculate α locally near each q and this can sometimes lead to an unexpected shape of $f(\alpha)$ as it is seen in Figure 1(b).

III. COMPUTER GENERATED DATA

First we shall consider a few examples of signals associated with some well-known processes for which the exact theoretical results are available. Our objective is to confront the outcomes of the analyzed methods against theory and detect advantages or disadvantages of each of the two procedures. Our analysis of artificial data concentrates on several important issues regarding the performance of MFDFA and WTMM:

- method's ability of correctly identifying monofractal or multifractal character of signals
- method's precision in evaluating $f(\alpha)$ spectra that agree with respective theoretical predictions
- stability of results across different variants of MFDFA (different polynomials) and of WTMM (different wavelets)
- stability of results across different realizations of a given stochastic process
- method's ability of providing one with correct results for short signals
- quality of scaling in $F_q(s)$ and $Z(q,s')$ and sensitivity of results to distinct choice of a fitting range of s or s'.

For the sake of consistency, we did not apply WTMM to original signals but rather to their integrated versions; this allowed us to compare the results of WTMM with the ones of MFDFA which in fact also analyze the integrated signal profile $Y(j)$ instead of $x(j)$ (see Eq. (1)). In order to be able to compare the results from both the F_q and the Z function, we also have to derive

$$|s'Z(q,s')|^{1/q} \sim {s'}^{h(q)}. \tag{13}$$

It is noteworthy that for the data analyzed here we deal with the two main possible sources of multifractality: the nonlinear temporal correlations and the broad probability density functions. Finally, we have to mention that an earlier approach to a comparison of MFDFA and WTMM [22] which was only briefly sketched there, showed that the former method can provide one with the results being in a better agreement with theoretical predictions than does the latter one. However, such a comparison was not a central issue of the cited work which was rather concentrated on the performance of MFDFA itself. Here we present a more thorough study on this subject.

A. Monofractal signals: Brownian motion

We start our comparative study with testing each method's ability of identifying and quantifying monofractal data. This is of great importance since in many practical situations the question which is usually addressed first is whether data under study is mono- or multifractal. In general, even if a method works satisfactorily well for very long signals, it may happen that for typical experimental time series the finite-size effects would lead to broadening of the $f(\alpha)$ spectra which are no longer point-like and this, obviously, may cause a spurious detection of multifractality. We would prefer a method which works more robust in such situations.

1. Classical Brownian motion

The first data type which we investigate is a simple case of a monofractal time series represented by the classical Brownian motion with the Hurst exponent $H = 0.5$. This process can be classified as stochastic with the stationary, independent and Gaussian-distributed increments. In order to obtain statistically significant results we carry out calculations on $K = 10$ independent realizations of this process. Theoretical spectrum consists here of one point localized at $\alpha = 0.5$ and $f(\alpha) = 1$ (Eq.(5)).

Uppermost panel of Figure 2 shows exemplary plots of the fluctuation function (Eq. (4), open symbols) and the rescaled partition function (Eq. (13), filled symbols) for a single realization of the process and for a few different values of the Rényi parameter q. As it can be seen, high absolute values of q typically correspond to plots with worse scaling, while small $|q|$'s are associated with plots exhibiting more clear power-law shape. This observation is valid for both MFDFA and WTMM, but in this particular case of a Brownian process, scaling for $q \ll 0$ is worser in WTMM than it is in MFDFA. This may cause some ambiguity in choosing a plot range for which the fitting procedure according to Eq. (13) is applied. This ambiguity can affect determining $\tau(q)$ and thus can introduce undesired values of $\alpha \neq 0.5$.

Taking all independent process realizations into our consideration, we derive the mean multifractal spectra

$$\overline{\tau(q)} = \sum_{k=1}^{K} \tau^{(k)}(q), \tag{14}$$

where the average is taken over all individual data samples. The so-calculated spectra (symbols) can be seen in bottom part of Figure 2 together with the theoretical linear spectrum (solid line). We applied the third derivative of a Gaussian (ψ^3) which is orthogonal, thus insensitive, to quadratic trends in a signal. For consistency, in MFDFA we chose polynomials $P^{(2)}$ (MFDFA(2)) and therefore we were also able to remove trends up to quadratic one.

An issue which has to be examined in this context is the range of q used in the analysis. On the one hand, it should be as wide as possible in order for the method to be capable of detecting even subtle multifractal effects in a signal. Thus, by taking an extremely narrow range of the Rényi parameter one might see a false, almost point-like $f(\alpha)$ even for a signal actually comprising a variety of singularities of different strength. On the other hand, taking a too large $|q|$ can produce statistically meaningless results based on an insufficient number of time series points. Figure 3 shows how the mean singularity spectra $\overline{f(\alpha)}$ calculated from $\overline{\tau(q)}$ according to formula (11) for the classical Brownian motion depend on q-range used: $-3 \leq q \leq 3$ (top), $-5 \leq q \leq 5$ (middle) and $-10 \leq q \leq 10$ (bottom). The most striking feature is a broad $\overline{f(\alpha)}$ calculated by means of WTMM (right column) as compared to its MFDFA counterpart (left column). It is interesting that only MFDFA gives a perfect identification of monofractality for the most narrow interval of $|q| \leq 3$, while WTMM does not. In the middle panels we see that while MFDFA still offers the spectrum that can approximately be considered a single point, WTMM shows $\overline{f(\alpha)}$ of a significant non-zero width $\Delta\alpha := \alpha(q_{\min}) - \alpha(q_{\max})$ that can even suggest a sort of multifractal scaling. By extending q up to ± 10, WTMM completely fails: the shape of the corresponding singularity spectrum becomes evidently multifractal. In contrast, despite its parabollic shape, $f(\alpha)$ for MFDFA is still defined on a relatively narrow $\Delta\alpha$ not allowing us to erroneously assume a multifractal character of the underlying process. In each panel, standard deviations of $\overline{f(\alpha)}$ are denoted by horizontal and vertical error bars.

There is no simple and straightforward explanation of how such a discrepancy between MFDFA and WTMM does occur. We have already seen in Figure 2 some problems with scaling of the partition function $Z(q, s')$ for q's distant from zero. However, this lack of an ideal power-law behaviour cannot fully account for the observed strong deviation of $f(\alpha)$ from its theoretically predicted form. This is because we carried out analogous calculations for a few different possible intervals of scales in which the fitting of $Z(q, s')$ was done according to Eq.(13), and in each case we eventually arrived at the qualitatively similar $f(\alpha)$ spectra. Another source of error can potentially be a poor statistics of data. Let us rewrite Eq. (10) in the following form

$$Z(q, s') = \sum_{l \in L(s')} \Theta(s')^q \tag{15}$$

and then let us define an effective number of maxima used in the calculation of $Z(q, s')$ for a fixed q and s' and express it by a fraction of the total number of detected maxima:

$$R^{(q)}_{\mathrm{WTMM}}(s') = \frac{1}{\Lambda} \ \min \#\{l \in L(s') : \sum_{l} \Theta(s')^q \geq 0.9 \cdot Z(q, s')\}, \tag{16}$$

where l and $L(s')$ have the same meaning as in Eq.(10) and $\Lambda = \#L(s')$. We also define a similar quantity for MFDFA:

$$R^{(q)}_{\mathrm{MFDFA}}(n) = \frac{1}{2M_n} \min \#\{\nu : (\frac{1}{2M_n} \sum_{\nu} [F^2(n, \nu)]^{q/2})^{1/q} \geq 0.9 \cdot F_q(n)\}, \tag{17}$$

where ν, M_n and F^2 are the same as in Eq.(3). Both these quantities are presented in Figure 4 for three choices of $q < 0$ and for a few different process realizations. As the plots show, for $q = -3$ and $q = -5$ both the estimates of $Z(q, s')$ and of $F_q(n)$ are based on a significant fraction of data for a vast majority of s' or n values. In contrast, for $q = -10$ the statistics is evidently poorer and might be considered unsatisfactory. In this case a too small fraction of the number of maxima (even < 10 maxima in absolute numbers) contributes to the scaling functions $F_q(n)$ and $Z(q, s')$ and thus they describe only the scaling properties of a few largest events instead of the properties of the whole signals. Curiously, despite the fact that both $R^{(q)}_{\mathrm{MFDFA}}$ and $R^{(q)}_{\mathrm{WTMM}}$ are statistically significant for $q = -5$ and $q = -3$, the output of MFDFA and WTMM is completely different. Consistently, qualitatively similar findings were also obtained for the other types of monofractal processes studied in this work. Thus we are justified to conclude that data statistics cannot be among principal sources of discrepancy in precision of both methods.

Based on these outcomes, from now on we will restrict our analysis to $-5 \leq q \leq 5$. We sample this parameter with $\Delta q = 0.1$ frequency for $|q| \leq 3$ and with $\Delta q = 0.5$ for $|q| > 3$.

The above discussion might indicate that a problem with the incorrect quantifying monofractal processes by WTMM as compared to MFDFA can rather be inherent to the WTMM procedure. For example, it may require significantly longer time series than does the detrended fluctuation method in order to obtain a good convergence in Eq. (10) for larger $|q|$'s. Therefore, in order to investigate how the methods work in respect to sample size, for the same type of Brownian motion we create sets of time series of different lengths ($N = 15,000$, $N =$

$65,000$, $N = 130,000$ data points). As Figure 5 shows, we observe a noticeable N-dependence of $\overline{f(\alpha)}$ especially for WTMM: the longer the time series, the better agreement with theory. It can also be seen that for smaller N the spectra produced by WTMM are much more unstable in terms of standard deviations than are the spectra for MFDFA. Obviously, standard deviations reveal also a strong dependence on N. Thus, for e.g. $N = 15,000$, $f(\alpha)$ for a single process realization is likely to falsely indicate multifractality and temporal correlations (persistence or antipersistence) in a completely random, uncorrelated signal. MFDFA seems to be more powerful here since even for short signals the standard deviations are acceptably small and the maximum of the average spectrum lies almost ideally at $\alpha = 0.5$. In contrast, for the signals as long as $N = 130,000$, WTMM provides us with the results that are not satisfactory. Perhaps, for much longer signals of length exceeding 10^6 data points, the situation would improve but, from a practical point of view, empirical signals of such a length are rarely available. This strongly favours MFDFA as a monofractality detector.

Next, we expect the results of an analysis to be insensitive as much as possible to a choice of the detrending polynomial $P^{(l)}$ in MFDFA and of the Gaussian derivatives $\psi^{(m)}$ in WTMM. Any significant dependence would limit robustness of a method since in the case of a real financial market one does not know a priori which polynomial or which wavelet function can be optimal. Figure 6 shows the mean singularity spectra $\overline{f(\alpha)}$ obtained by using MFDFA(l) with $l = 1, 2, 3, 4$. For $P^{(1)}$ we do not observe exactly single-point spectrum but rather a very narrow parabola. By increasing l we see decreasing $\Delta\alpha$, the effect that is easily understandable: higher-order polynomials can better detrend the data. It seems that even $P^{(2)}$ works sufficiently well in the present case. Successfully, in all cases the location of the spectra agrees perfectly with the expected $H = 0.5$. The corresponding results for WTMM ($m = 1, 2, 3, 4$) are collected in Figure 7. We see that although maxima of $\overline{f(\alpha)}$ are situated correctly, the spectra are definitely too wide to be considered monofractal. The largest discrepancy between these results and the theory is for $\psi^{(1)}$, while for the higher-order derivatives the spectra are comparable in their widths (although still far from being monofractal). It is also noteworthy that starting from $m = 2$, the standard deviations tend to increase with increasing derivative order. For MFDFA, where the standard deviations are much smaller, such a behaviour is not observed.

2. *Fractional Brownian motion*

In contrast to the above uncorrelated ordinary Brownian motion, the fractional Brownian motion with $H \neq 0.5$ can serve as an example of a monofractal process with temporal correlations. Impact of these correlations on the results of MFDFA and WTMM can be evaluated from Figures 8-10. The two following cases are discussed: an antipersistent process with $H = 0.3$ and a persistent one with $H = 0.75$. Comparison of the $f(\alpha)$ spectra in Figures 8 and 9 calculated for different $P^{(l)}$ (MFDFA, left columns) and $\psi(m)$ (WTMM, right columns) leads to esentially similar conclusions as in the case of $H = 0.5$.

(a) In each case MFDFA acts excellently for the antipersistent process: it shows clearly a complete lack of multiscaling. In the persistent case the spectra are less perfect, although they still cannot be erroneously considered multifractal. As compared to MFDFA, $\Delta\alpha$ for WTMM is large and thus the corresponding WTMM spectra fail to reflect the actual monofractality of the signals. However, for high Gaussian derivatives like $\psi^{(4)}$ WTMM spectrum can be very narrow and its $\Delta\alpha$ can potentially be used as an indicator of possible monofractality of an analyzed signal.

(b) MFDFA provides us with the correct value of H in both the persistent and the antipersistent case. From this point of view WTMM also works well as regards the average spectra, but it turns less reliable for the individual signals.

(c) The average outcomes of MFDFA can be accounted stable across their different-order variants, while WTMM tends to work better if one uses higher Gaussian derivatives ($m \geq 3$).

It should be stressed that we assume no a priori knowledge of the processes underlying the data. This, for example, distinguishes our analysis from the one carried out by authors of ref. [24] who also applied WTMM to the fractional Brownian motion with $H = 0.3$. They took an advantage of the knowledge that the analyzed process had to reveal monofractal scaling and, accordingly, they were able to fit a straight line to the computed $\tau(q)$. As a consequence, they obtained the exact single-point $f(\alpha)$. However, for data with unknown properties one has to calculate spectra by local fits and for WTMM this leads to a dispersion of α's even for monofractal processes. On the other hand, authors of ref. [22] carried out an MFDFA analysis based on three types of Brownian motion ($H = 0.25$, $H = 0.5$, $H = 0.75$) and they obtained similar results to the ones presented here. Even more, they were able to show that MFDFA can be reliable even for $|q| > 10$.

Finally, we take a look at the results obtained for different time series lengths (Figure 10). For the comparison purpose we choose $l = 2$ and $m = 3$. For $H = 0.3$ we see that while MFDFA gives us a narrow spectrum even for a signal as short as $N = 15,000$ with increasing its accuracy with increasing N, the WTMM method occurs totally unreliable for shorter signals. The case of $H = 0.75$ does not differ much from the previous one but now MFDFA slightly looses its perfect accuracy and does not converge so well to a monofractal spectrum with increasing N. This is especially evident if a broader range $|q| \leq 10$ is used (not shown). Broadening of the MFDFA spectrum is a gradual process that becomes more evident for persistent signals with $H \gg 0.5$. It is worth mention-

ing that for both methods and for all N the maxima of $\overline{f(\alpha)}$ point at the correct values of α.

B. Bifractal signals: Lévy processes

The second interesting class of processes which are of high practical utility are the stable Lévy processes. Their applications range from physiology to financial markets; in the latter case it is hypothesized that the modification of this kind of processes, i.e. the truncated Lévy flights (with the exponent-suppressed Lévy distribution tails) describes the price fluctuations of stocks. The scaling exponent $\tau(q)$ for the truncated Lévy flights (with the Lévy parameter α_L) and for non-Lévy signals with the tails obeying the power law distribution $P(x) \sim x^{-(\alpha_L+1)}$ can be expressed by [22, 28]

$$\tau(q) = \begin{cases} q/\alpha_L - 1 & (q \leq \alpha_L) \\ 0 & (q > \alpha_L) \end{cases} \tag{18}$$

and the associated singularity spectrum by

$$\alpha = \begin{cases} 1/\alpha_L & (q \leq \alpha_L) \\ 0 & (q > \alpha_L) \end{cases} \quad f(\alpha) = \begin{cases} 1 & (q \leq \alpha_L) \\ 0 & (q > \alpha_L) \end{cases} . \tag{19}$$

As these expressions show, signals with the truncated Lévy distributions are rather bifractal than multifractal [28]. From a dynamical point of view, the bifractal spectra or, more generally, the spectra revealing singularity in $\tau(q)$, can often be seen in systems exhibiting phase transitions like e.g. chaotic systems with intermittency [29, 30, 31, 32]. It should also be noted that in principle the moments higher than α_L do not exist at all, but as we consider the time series of finite lengths, we can also calculate $h(q)$ for $q > \alpha_L$. We chose a heavy-tailed distribution with $\alpha_L = 1.5$ and generated $K = 10$ time series of length $N = 250,000$ data points each. Examples of $F_q(s)$ and $|s'Z(q,s')|^{1/q}$ as well as of $\overline{\tau(q)}$ for MFDFA ($l = 2$) and for WTMM ($m = 3$) are shown in Figure 11. Scaling of $F_q(s)$ worsens for large positive q's (triangles down), while scaling of $|s'Z(q,s')|^{1/q}$ proves weak for strongly negative q's.

Figure 12 presents results for different variants of MFDFA and WTMM. It is interesting to note that MFDFA (left column) presents a good agreement with theory near the bifractal points (Eq.(19)) where there are two dense clusters of symbols. Unexpectedly, for each $P^{(l)}$ we also observe a continuous transition between these clusters. However, such a spurious transition is rather inevitable for real data supposed to exhibit two different linear regimes of $\tau(q)$ (see also [25, 30] for other examples of spectra displaying an analogous transition). Main difference between spectra for different values of l is that the cluster at $\alpha = 1/\alpha_L$ tends to be better localized for $l > 1$. On the other hand, for all Gaussian derivatives in WTMM we observe roughly the same artificial transition as for MFDFA, but there is also an additional spurious arm of the spectrum for large α (i.e. strongly negative q) that effectively disperses the spectrum beyond its theoretical prediction. This arm can be a consequence of weak scaling in Figure 11 that in turn can be a consequence of inherent problems with correct calculation of the multifractal spectra for $q < 0$. In this case estimation of $F_q(n)$ or $Z(q,s')$ might be strongly biased by the existence of very small values in time series which can be largely amplified if their negative exponents are considered; thus they can dominate the results completely [33, 34]. Unfortunately, this situation only slowly improves with a time series length so that some other, more refined techniques are required [34].

Influence of N on the results can be inferred after inspecting Figure 13. Apart from the longer error bars for $N = 100,000$, for both methods the spectra for longer signals are smoother near the theoretical points, which reflects more reliable fits according to Eq.(4) and Eq.(13).

C. Multifractal signals: binomial cascades

In this subsection we present results for processes which are inherently multifractal, i.e. binomial multiplicative cascades [22, 24]. Processes of this kind are commonly used to model fluid turbulence and due to the recently-formulated hypothesis of similarity between the turbulence and the evolution of financial markets [41], they are more and more often applied in econophysics [35, 36, 38, 39, 40].

1. Deterministic case

Let us consider a probability measure μ_0 distributed uniformly on interval $[0,1]$ and two numbers m_0, m_1 such that $m_0 + m_1 = 1$. In the first step we uniformly spread a fraction m_0 of total mass on the left subinterval $[0,1/2]$ and a fraction m_1 on the right subinterval $[1/2,1]$. In the second and subsequent steps we repeat this procedure for each of the subintervals using in each step the same fractions m_0 and m_1 of the higher-level subinterval mass. In kth step, each subinterval j $(j = 1, ..., 2^k)$ can be labelled by a unique sequence $[\eta^{(j)}] = \eta_1^{(j)}\eta_2^{(j)}...\eta_k^{(j)}$, where $\eta_i^{(j)}$ is either 0 or 1. Thus, a measure of this subinterval is $\mu_k[\eta^{(j)}] = m_0^{k-n(j-1)} m_1^{n(j-1)}$, where $n(j)$ denotes a number of unities in the binary representation of j. This construction leads to preservation of the total mass on subinterval $[0,1]$, i.e. the measure μ_k is conservative $\sum_j \mu_k[\eta^{(j)}] = 1$. In the limit $k \to \infty$ the measure μ_k goes to binomial measure μ.

The above-defined procedure generates a binomial cascade that after $k_{\max}$ steps can be represented by a time series $\{x_j\}_{j=1}^N$ of length $N = 2^{k_{\max}}$ such that

$$x_j = a^{n(j-1)}(1-a)^{k_{\max}-n(j-1)}, \tag{20}$$

where $a = m_0$ and $a \in (0.5, 1)$. The resulting signal possesses singularities of strength depending on the param-

eter a and, for a significantly less than 1, its multifractality comes mostly from the temporal correlations (for $a \to 1$ the broad probability distribution of x_j also contributes much). The analytical expression for the scaling exponent and for the singularity spectrum can both be derived straightforwardly [22]:

$$\tau(q) = -\frac{-\ln[a^q + (1-a)^q]}{\ln(2)} \tag{21}$$

$$\alpha = -\frac{1}{\ln(2)} \frac{a^q \ln(a) + (1-a)^q \ln(1-a)}{a^q + (1-a)^q} \tag{22}$$

$$f(\alpha) = -\frac{q}{\ln(2)} \frac{a^q \ln(a) + (1-a)^q \ln(1-a)}{a^q + (1-a)^q} - \frac{-\ln[a^q + (1-a)^q]}{\ln(2)}. \tag{23}$$

In order to check how the MFDFA and WTMM methods work for different values of the parameter a, we consider time series constructed for $a = 0.55$ (a relatively smooth signal), for $a = 0.75$ (existence of sharp singularities) and for an intermediate case of $a = 0.65$. It comes from the definition (Eq. (20)) that by increasing a we enhance the role of heavy-tailed p.d.f. of $\{x_j\}$ and we also make the multifractality richer (larger $\Delta\alpha$). Conversely, for $a \to 0.5$ the theoretical singularity spectrum tends to a monofractal one. We perform calculations on time series of length $N = 131,072$, i.e. in each case we stop the cascade-generating procedure at $k_{\max} = 17$. Unlike for the Brownian and Lévy processes, here due to the deterministic nature of the cascades under study we create only one time series for each value of the parameter a. Figure 14(a) shows exemplary plots of $F_q(s)$ for MFDFA ($P^{(2)}$) and $|s'Z(q,s')|^{1/q}$ for WTMM ($\psi^{(3)}$). Globally for a large range of s the scaling is relatively good despite the local fluctuations. Similar results can be obtained by using different polynomials in MFDFA or different Gaussian derivatives in WTMM (not shown here). As regards $\tau(q)$ shown in the panels (b) and (c), the estimated spectra resemble the theoretical one with the WTMM-based spectrum presenting almost perfect agreement with theory.

The singularity spectra computed for distinct variants of MFDFA and WTMM are compared in Figure 15 with the ones theoretically derived according to Eq. (22) and Eq. (23). Interestingly, for $a = 0.55$ the only case in which we observe an agreement between theory and numerical estimates is for WTMM with $\psi^{(1)}$ (top right panel). For other wavelets the spectra deviate in either α or in $f(\alpha)$ and the same happens for all the analyzed polynomials of MFDFA (top left). A much better performance of WTMM is seen for $a = 0.65$ (middle right) where only $\psi^{(2)}$ does not reproduce the theoretical spectrum, while by using the other Gaussian derivatives we get the correct outcomes. MFDFA offers us the $f(\alpha)$ spectra that slightly deviate from the expected one for positive values of the Rényi parameter q (corresponding to large signal fluctuations, left arms in middle-left panel of Figure 15) but their shape does not depend on the polynomial $P^{(l)}$. Similar conclusions regarding MFDFA can be formulated for $a = 0.75$ (bottom left). In contrast, WTMM seems to be unable to cope with the latter kind of data for small (negative) q's (small signal fluctuations): it significantly underestimates width of the spectrum on higher-α side which is most strikingly evident for $\psi^{(3)}$ and $\psi^{(4)}$ (bottom right). An agreement between theory and practice is reached only for positive q's except the wavelet $\psi^{(2)}$. In general, as regards the whole spectra, for $a = 0.75$ the wavelets $\psi^{(1)}$ and $\psi^{(2)}$ behave more reliably than the remaining ones. It is also noteworthy that for all the studied values of a, the MFDFA results are remarkably independent of the polynomial choice, the property that cannot be attributed to WTMM and the choice of a wavelet.

For next point of our analysis we prepare time series of different lengths $N = 16,384$, $N = 65,536$ and $N = 131,072$ in order to investigate how smaller N can affect the reliability of calculations as compared to long signals. Based on Figure 15, for each a we choose a wavelet with the best performance: $\psi^{(1)}$ for $a = 0.55$, $\psi^{(3)}$ for $a = 0.65$ and $\psi^{(2)}$ for $a = 0.75$. MFDFA is represented by the polynomial $P^{(2)}$. Figure 16 collects plots of the corresponding singularity spectra; in a sharp contrast to Figures 10 and 13, in the present case the spectra are practically not sensitive to time series length in a wide range of N. At the end, we note that the outcomes presented here for MFDFA agree with the ones from reference [22].

2. Stochastic case

The above-described procedure can be generalized in a number of ways, e.g. by increasing the number of equal-size subintervals into which an interval is splitted at each cascade stage k and/or by randomizing the mass allocation among the subintervals. This latter way is especially appealing because it allows one to eliminate the unrealistic determinism of the previous example. Even more general models that can be related to financial data are available in literature (see e.g. [37, 48, 49]) but within the scope of the present work it is sufficient that we concentrate exclusively on some simplest stochastic cascade processes of multifractal nature. Proceeding along this line, we preserve the binomial character of the cascade but we replace the conservative measure with a multiplicative one that allows the multipliers m_i to be independent, identically distributed random variables drawn from a specific distribution. Now the total mass on interval $[0, 1]$ is preserved only in a statistical sense: $E(\sum_i m_i) = 1$. It has been shown that a resulting process produces signal with multifractal properties [36, 50, 51]. Random multiplicative cascades, and especially their iterative versions [39, 52], are in practice much more interesting than

their deterministic counterparts due to the fact that they are able to mimic stochastic character of financial volatility fluctuations over time. Here we discuss the singularity spectra of three common versions of such processes, i.e. Poisson, Gaussian and gamma multiplicative cascades.

a. Log-Poisson cascade Let us start with a discrete cascade characterized by the multipliers $m(\eta_1, ..., \eta_k)$ such that $M(\eta_1, ..., \eta_k) := -\log m(\eta_1, ..., \eta_k)$ have Poisson distribution

$$p(x) = \frac{e^{-\gamma}\gamma^x}{x!} \ . \tag{24}$$

At a stage k, an interval j has the mass

$$\mu_k([\eta^{(j)}]) = m(\eta_1)m(\eta_1, \eta_2) \cdot ... \cdot m(\eta_1, ..., \eta_k) \tag{25}$$

and therefore

$$-\ln \mu_k = \sum_i M(\eta_1, ..., \eta_i) \ . \tag{26}$$

The sum on the right-hand side is also Poisson-distributed with $\gamma \to k\gamma$ in Eq.(24) and this leads to the following formula for the singularity spectrum [36]

$$f(\alpha) = 1 - \frac{\gamma}{\ln 2} + \alpha \log_2(\gamma e/\alpha). \tag{27}$$

This spectrum assumes its maximum at $\alpha_0 = \gamma$ and has negative values for $\alpha \gg \gamma$ and for $\alpha \to 0$ if $\gamma > \ln 2$. Based on the above-described generating procedure we create a time series representing the $k = 17$th stage of the log-Poisson binomial cascade and by applying MFDFA and WTMM we estimate $f(\alpha)$. Figure 17 collects the results obtained with different variants of wavelets $(\psi^{(1)}, ..., \psi^{(4)})$ and polynomials $(P^{(1)}, ..., P^{(4)})$.

For WTMM (right-hand side) we observe the mean spectra whose increasing arms generally agree with the spectrum of Eq. (27) but, on the contrary, the decreasing arms completely fail to comply with theory. MFDFA works substantially better than WTMM for $\alpha > \alpha_0$, even if it does not reproduce the theoretical curve ideally after averaging $f(\alpha)$ over all 10 individual cascade realizations. This resembles the results for the deterministic cascades with $a = 0.75$ (Figure 15), where we also noticed problems with estimating $f(\alpha)$ for $\alpha > 1$ by means of WTMM. Therefore, this seems to be a more general issue of dealing with signals comprising relatively smooth singularities associated with high α's. Both for MFDFA and for WTMM, significant error bars on both coordinates reveal strong instability of the calculated spectra which vary from sample to sample. Figure 18 displays $\overline{f(\alpha)}$ for different time series lengths (different k's). Again, MFDFA gives better results in respect to Eq. (27) even for relatively short signals than does the wavelet-based method. These outcomes for the log-Poisson cascades collected in Figures 17 and 18 qualitatively resemble the results of ref. [22] for the same type of data.

b. Log-gamma cascade As another example of a multiplicative cascade we investigate a process with the multipliers whose logarithms are taken (with minus sign) from the gamma p.d.f.

$$p(x) = \beta^\gamma x^{\gamma-1} e^{-\beta x}/\Gamma(\gamma) \tag{28}$$

where $\beta, \gamma > 0$. A sum of k *i.i.d.* random variables with such distributions is also a gamma distribution with $\gamma \to k\gamma$. Following [36] we can write the analytical form of the $f(\alpha)$ spectrum

$$f(\alpha) = 1 + \gamma \log_2(\alpha\beta/\gamma) + (\gamma - \alpha\beta)/\ln 2 \tag{29}$$

which reaches its maximum for $\alpha_0 = \gamma/\beta$.

The plots in Figures 19 and 20 qualitatively resemble those from Figure 17 and 18 and, at least in part, similar conclusions can be drawn in the present case as it was for the log-Poisson one. Though, we note that at the decreasing part of the $f(\alpha)$ curves the error bars indicate extreme unstability of the computed spectra, suggesting that here neither of the two methods can be trusted for $q < 0$. This is caused by the fact that in this case plots of $F_q(n)$ and of $|s'Z(q, s')|^{1/q}$ (not shown) present so weak scaling that even a small change of the fitting range of n and s' profoundly affects $f(\alpha)$. (See also the respective discussion related to the Lévy processes.)

c. Log-normal cascade Finally, we consider the multipliers whose logarithms are taken from a Gaussian distribution

$$p(x) = \frac{1}{(2\pi\sigma^2)^{1/2}} e^{-(x-\lambda)^2/2\sigma^2}. \tag{30}$$

The singularity spectrum for a log-normal cascade

$$f(\alpha) = 1 - \frac{1}{2\ln 2\sigma^2}(\alpha - \lambda)^2 \tag{31}$$

has a maximum for $\alpha_0 = \lambda$ and extends over $-\infty < \alpha < +\infty$ due to a possible lack of mass conservation. This theoretical spectrum has to be compared with spectra derived from time series by means of the MFDFA and WTMM methods. Figure 21 present such a comparison for the polynomials $P^{(1)}, ..., P^{(4)}$ used in different variants of MFDFA (left column) and for a few Gaussian derivatives $\psi^{(1)}, ..., \psi^{(4)}$ used in WTMM (right column). It is clear that, as regards the mean spectra calculated from 10 independent realizations of the cascade and a range of α's for which $f(\alpha) > 0$, both methods give results that for a log-normal cascade are much closer to theoretical predictions than it was for the two cascades discussed above. This is particularly evident for the decreasing part of the spectra, despite the existing deviations for $\alpha \geq 1.5$. We observe a satisfying stability of the mean spectra across different variants of the methods and we do not notice any significant differences between the spectra produced by MFDFA and by WTMM except the fact that the standard deviations of data points tend to be larger for WTMM than for MFDFA. Also if we look at

the average spectra evaluated for different signal lengths (Figure 22) we see that the results differ mainly in stability across process realizations. In general, the standard deviations in α are relatively small while they are large in $f(\alpha)$; they are also much smaller in the increasing parts of the spectra than in the decreasing ones.

IV. STOCK MARKET DATA

In this Section we apply both methods of the multifractal analysis to real data from a stock market. Let us denote by $P_s(t_i)$ the price of an asset s at the ith consecutive time instant (t_i may in general not be equally spaced in time). We create a time series of logarithmic price increments $p_s(t_i) = \ln(P_s(t_{i+1})) - \ln(P_s(t_i))$, where $i = 1, ..., N$. The difference between our price increments $p_s(t_i)$ and the returns is that t_i denote the moments of transactions instead of the moments of constant-frequency data sampling. It should be noted that such a choice of data, motivated by our recent interest [20], leads to the qualitative results that can be also drawn for the standard returns.

We carried out the calculations for the time series representing 30 stocks comprised by Deutsche Aktienindex (DAX) and for the ones representing 30 Dow Jones Industrial stocks (DJIs) in the period 12/01/1997 - 12/31/1999 [53]. Each time series under study had different length ranging from 63,000 (Karstadt) to 2,236,000 (The Walt Disney Co.) data points. In a preliminary stage the data was preprocessed in the following way: we removed all overnight price increments (they were characterized by different statistical properties than the rest of the increments) and we also removed all the constant price intervals with more than 20 consecutive zeros (the MFDFA procedure requires a compact support of the signal in order to avoid the divergence of F_q for $q < 0$ and, thus, in order to improve scaling; fortunately, the wavelet-based method is insensitive to the presence of such zero intervals, because it only deals with the maxima of T_ψ). Due to the fact that the analyzed data is characterized by both the broad probability density function and by the correlations in the temporal domain, we additionally estimate the contribution of each multifractality source by calculating $f(\alpha)$ for the original and for the randomly reshuffled signals. Obviously, in the latter case the spectra may depend only on p.d.f.'s.

We start with the results obtained for the DAX stocks. Figure 23(a) shows the fluctuation function $F_q(s)$ and the rescaled partition function $|s'Z(q,s')|^{1/q}$ for a randomly selected stock. Good-quality scaling for a broad range of s can be easily seen for different q's. Figure 23(b) and 23(c) show $\tau(q)$ averaged over all 30 stocks, while Figure 24 displays the related mean singularity spectra (open circles). As this Figure documents, maxima of $\overline{f(\alpha)}$ are localized approximately at $\alpha = 0.52$ (MFDFA) and $\alpha = 0.53$ (WTMM) which suggests a weak trace of linear correlations in data. The main difference between the spectra obtained by each of the two methods is that their widths are different: MFDFA produces a thinner spectrum than does WTMM. We can say that for the stock market data WTMM detects a richer multifractality than does MFDFA. This also refers to the reshuffled signals, which of course do not show any linear correlations and their maxima are located precisely at $\alpha = 0.5$. For the DJI stocks (Figure 26, open circles), $\overline{f(\alpha)}$ has a maximum at $\alpha = 0.51$ (MFDFA) and $\alpha = 0.53$ (WTMM), while for the reshuffled signals a maximum is at $\alpha = 0.5$, which is consistent with the corresponding results for the German market. This consistency is also seen in the relation between widths of the real-data spectra derived by MFDFA and by WTMM. In Figure 26 both methods give spectra that on average are narrower than for the German stocks in Figure 24, while the opposite refers to $\overline{f(\alpha)}$ for the reshuffled signals (filled squares). For DAX, it is even disputable whether the reshuffled-data spectra may be considered multifractal. However, significant standard deviations of data points (denoted by error bars in Figures 24 and 26) might question validity of these observations. Thus, we are not justified to infer any decisive conclusions about similarity or dissimilarity of the outcomes of MFDFA and WTMM for our financial signals. (This can be compared with the outcomes of an analysis of river run-off and precipitation data in ref. [10], where both methods produced results resembling each other.)

Table 1 summarizes the results for the original and for the randomized signals coming from both markets. In each case the width $\Delta\alpha$ is larger for an original than for a randomized signal which is due to the existence of strong nonlinear correlations. A more careful inspection of Table 1 allows us to state that MFDFA identifies the temporal correlations as the principal source of multifractality ($\Delta\alpha_{\rm rand} \ll \Delta\alpha$). The outcomes of WTMM also go in this direction but they are burdened with larger statistical uncertainity.

V. CONCLUSIONS

Our aim was to verify which of the two existing modern methods of detecting multifractality, MFDFA or WTMM, gives more reliable results when applied to a few specific sorts of data. In order to quantify their behaviour we tested these methods on computer-generated time series with the exactly known fractal properties and then we performed calculations with an exemplary real data from a stock market. Our results indicate that from a global point of view the Multifractal DFA works better in the majority of situations presented here. First of all, as our examples of the fractional Brownian motion and the truncated-Lévy process show, MFDFA is more reliable in properly detecting monofractal and bifractal behaviour than is the wavelet-based method. In such a case WTMM can spuriously suggest multifractality if a too wide range of the Rényi parameter is used. Thus, in

an analysis of a signal with unknown fractal properties, if one has to determine whether it is monofractal or multifractal, one faces a fundamental problem of choosing a reliable range of q. What makes finding a solution to this problem difficut is that for such a process one cannot assume which values of q give a correct result and which do not. From this perspective, MFDFA can be a much better option due to the fact that one may apply it more automatically, without paying too much attention to a choice of q. For obtaining reliable results it is sufficient if q are not chosen extremely large. Performance of both methods worsens with decreasing time series length, but typically the DFA-based method works better than WTMM also for shorter signals (of length $N \sim 10^4$).

For actual multifractal data both MFDFA and WTMM are able to roughly assess $f(\alpha)$ at least for $q > 0$, while taking $q \ll 0$ into consideration is hazardous, especially for WTMM as our discussion on binomial cascades shows. A serious advantage of MFDFA over WTMM is a better stability of the former in respect to different $P^{(l)}$'s; changing the wavelet $\psi^{(m)}$ can substantially affect the outcomes of WTMM (Figures 15, 17, and 19). Furthermore, our findings indicate that WTMM performs poorly with signals comprising singularities of strength $\alpha > 1$ (e.g. the deterministic binomial cascades, the log-Poisson and the log-gamma cascades): In this case it fails to detect the smoothest ones. This might be related to the fact that WTMM has inherent problems with such signals [24, 25]: By construction, in order for WTMM to be capable of detecting the singularities of strength $m_{\min}$, the corresponding wavelet has to be at least $\psi^{(m_{\min})}$. In consequence, if one is interested in investigating a broad range of singularities including the ones for $\alpha \gg 1$, one has to choose a high order Gaussian derivative $\psi^{(m)}$ or has to switch to MFDFA otherwise. Finally, accuracy of MFDFA is sensitive to the presence of linear correlations in data. Our results for the fractional Brownian motion show that the more persistent the signal, the worse MFDFA performance. But even for $H \gg 0.5$ it overperforms its wavelet competitor, as it does also for data with broad p.d.f. (Figures 12 and 15).

However, despite these observations that are in favour of MFDFA, we do not disregard the wavelet-based method completely. For example, it can still be successfully used for multifractal signals provided that one is principally interested in fluctuations associated with moderate positive q's. As our analysis reveals, for such q's in a number of model situations WTMM acts as well as does MFDFA. If one is careful enough to confine an analysis to some small range of $|q|$ for which scaling of $Z(q, s)$ is particularly good and based on a good statistics of data, then the increasing arms of the $f(\alpha)$ spectra for monofractal signals can be defined on a narrow range of α. Thus, if compared with some benchmark like the fractional Brownian motion, the results can indicate the character of the signals correctly. WTMM can also be a good alternative to MFDFA for signals which are defined on a non-compact support and comprise a significant number of zeros. Furthermore, one has to keep in mind that across our analysis we applied only a single wavelet family of the Gaussian derivatives. Although these wavelets are particularly popular in studies of empirical signals, we cannot exclude a possibility that some other type of wavelets can act better if applied to WTMM. Finally, a caution is needed about susceptibility of WTMM several factors in its numerical implementation. These in particular involve noise in maxima-detecting wavelet transform computation at small scales and the related boundaries.

	DJI: MFDFA	DJI: WTMM	DAX: MFDFA	DAX: WTMM
$\Delta\alpha$	0.13 ± 0.05	0.25 ± 0.10	0.16 ± 0.05	0.26 ± 0.07
$\Delta\alpha_{\rm rand}$	0.04 ± 0.02	0.08 ± 0.02	0.02 ± 0.01	0.05 ± 0.02
$\Delta\alpha_{\rm rand}/\Delta\alpha$	0.30 ± 0.19	0.32 ± 0.15	0.16 ± 0.07	0.19 ± 0.09

TABLE I: Numerical results for the mean singularity spectra for the DAX and DJI stocks.

[1] C.-K. Peng, S.V. Buldyrev, S. Havlin, M. Simons, H.E. Stanley, A.L. Goldberger, Phys. Rev. E **49**, 1685-1689 (1994)

[2] S.V. Buldyrev, A.L. Goldberger, S. Havlin, R.N. Mantegna, M.E. Matsa, C.-K. Peng, M. Simons, H.E. Stanley, Phys. Rev. E **51**, 5084-5091 (1995)

[3] A. Arneodo, Y. d'Aubenton-Carafa, E. Bacry, P.V. Graves, J.F. Muzy, C. Thermes, Physica D **96**, 291-320 (1996)

[4] P.Ch. Ivanov, L.A.N. Amaral, A.L. Goldberger, S. Havlin, M.G. Rosenblum, Z.R. Struzik, H.E. Stanley, Nature **399**, 461-465 (1999)

[5] J.M. Hausdorff, Y. Ashkenazy, C.-K. Peng, P.Ch. Ivanov, H.E. Stanley, A.L. Goldberger, Physica A **302**, 138-147 (2001)

[6] S. Blesic, S. Milosevic, D. Stratimirovic and M. Ljubisavljevic, Physica A **268**, 275-282 (1999)

[7] E. Koscielny-Bunde, A. Bunde, S. Havlin, H.E. Roman, Y. Goldreich, H.-J. Schnellnhuber, Phys. Rev. Lett. **81**, 729 (1998)

[8] N. Kitova, K. Ivanova, M. Ausloos, T.P. Ackerman, M.A. Mikhalev, Int. J. Mod. Phys. C **13**, 217 (2002)

[9] K. Ivanova, H.N. Shirer, E.E. Clothiaux, N. Kitova, M.A. Mikhalev, T.P. Ackerman, M. Ausloos, Physica A **308**, 518 (2002)

[10] J.W. Kantelhardt, D. Rybski, S.A. Zschiegner, P. Braun, E. Koscielny-Bunde, V. Livina, S. Havlin, A. Bunde, Physica A **330**, 240-245 (2003)

[11] M. Pasquini and M. Serva, Economics Letters **65**, 275-279 (1999)

[12] K. Ivanova and M. Ausloos, Physica A **265**, 279-291 (1999)

[13] A. Bershadskii, Physica A **317**, 591-596 (2003)

[14] T. Di Matteo, T. Aste and M.M. Dacorogna, Physica A

324, 183-188 (2003)
[15] A. Fisher, L. Calvet and B. Mandelbrot, *Multifractality of Deutschemark / US Dollar Exchange Rates*, Cowles Foundation Discussion Paper 1166 (1997)
[16] N. Vandewalle and M. Ausloos, Eur. Phys. J. B **4**, 257-261 (1998)
[17] A. Bershadskii, Eur. Phys. J. B **11**, 361-364 (1999)
[18] K. Matia, Y. Ashkenazy and H.E. Stanley, Europhys. Lett. **61**, 422-428 (2003)
[19] P. Oświęcimka, J. Kwapień, S. Drożdż, Physica A **347**, 626-638 (2005)
[20] J. Kwapień, P. Oświęcimka, S. Drożdż, Physica A **350**, 466-474 (2005)
[21] Y. Ashkenazy, D.R. Baker, H. Gildor and S. Havlin, Geophys. Res. Lett. **30**, 2146 (2003)
[22] J.W. Kantelhardt, S.A. Zschiegner, E. Koscielny-Bunde, A. Bunde, S. Havlin and H.E. Stanley, Physica A **316**, 87-114 (2002)
[23] M. Ignaccolo, P. Allegrini, P. Grigolini, P. Hamilton, B.J. West, Physica A **336**, 595-622 (2004)
[24] J.F. Muzy, E. Bacry, A. Arneodo, Int. J. Bif. Chaos **2**, 245-302 (1994)
[25] A. Arneodo, E. Bacry, J.F. Muzy, Physica A **213**, 232-275 (1995)
[26] Z.R. Struzik, A. Siebes, *Wavelet Transform in Similarity Paradigm I*, CWI report, INS-R9802 (1998); Z.R. Struzik, A. Siebes, *Wavelet Transform in Similarity Paradigm II*, CWI report, INS-R9815 (1998)
[27] P. Manimaran, P.K. Panigrahi, J.C. Parikh, Phys. Rev. E **72**, 046120 (2005)
[28] H. Nakao, Phys. Lett. A **266**, 282-289 (2000)
[29] R. Badii, A. Politi, Phys. Scr. **35**, 243 (1987)
[30] D. Katzen, I. Procaccia, Phys. Rev. Lett. **58**, 1169-1172 (1987)
[31] P. Szépfalusy, T. Tél, A. Csordás, Z. Kovács, Phys. Rev. A **36**, 3525-3528 (1987)
[32] R. Artuso, P. Cvitanović, B.O. Kenny, Phys. Rev. A **39**, 268-281 (1989)
[33] L.V. Meisel, M. Johnson, P.J. Cote, Phys. Rev. A **45**, 6989-6996 (1992)
[34] M. Alber, J. Peinke, Phys. Rev. E **57**, 5489-5493 (1998)
[35] B.B. Mandelbrot, *Fractal and Scaling in Finance: Discontinuity, Concentration, Risk*, Springer Verlag (New York, 1997)
[36] L. Calvet, A. Fisher, B.B. Mandelbrot, *Large Deviations and the Distribution of Price Changes*, Cowles Foundation Discussion Paper 1165 (1997)
[37] J. Barral, B. Mandelbrot, Probab. Theory Rel. **124**, 409-430 (2002)
[38] T. Lux, *The Multi-Fractal Model of Asset Returns: Its Estimation via GMM and Its Use for Volatility Forecasting*, Univ. of Kiel, Working Paper (2003)
[39] T. Lux, *Detecting multi-fractal properties in asset returns: The failure of the 'scaling estimator'*, Univ. of Kiel, Working Paper (2003)
[40] Z. Eisler and J. Kertész, Physica A **343**, 603-622 (2004)
[41] S. Ghasghaie, W. Breymann, J. Peinke, P. Talkner and Y. Dodge, Nature **381**, 767-770 (1996)
[42] V. Plerou, P. Gopikrishnan, L.A.N. Amaral, M. Meyer and H.E. Stanley, Phys. Rev. E **60**, 6519-6529 (1999)
[43] P. Gopikrishnan, V. Plerou, L.A.N. Amaral, M. Meyer and H.E. Stanley, Phys. Rev. E **60**, 5305-5316 (1999)
[44] V. Plerou, P. Gopikrishnan, L.A.N. Amaral, X. Gabaix and H.E. Stanley, Phys. Rev. E **62**, R3023-R3026 (2000)
[45] S. Drożdż, J. Kwapień, F. Gruemmer, F. Ruf and J. Speth, Acta Phys. Pol. B **34**, 4293-4305 (2003)
[46] X. Gabaix, P. Gopikrishnan, V. Plerou, H.E. Stanley, Nature **423**, 267-270 (2003)
[47] T.C. Halsey, M.H. Jensen, L.P. Kadanoff, I. Procaccia, B.I. Shraiman, Phys. Rev. A **33**, 1141-1151 (1986)
[48] J.F. Muzy, E. Bacry, Phys. Rev. E **66**, 056121 (2002)
[49] E. Bacry, J.F. Muzy, Commun. Math. Phys. **236**, 449-475 (2003)
[50] B. Mandelbrot, A. Fisher, L. Calvet, *A Multifractal Model of Asset Returns*, Cowles Foundation Discussion Paper 1164 (1997)
[51] B. Mandelbrot, Pure Appl. Geophys. **131**, 5-42 (1989)
[52] L. Calvet, A. Fisher, J. Econometrics **105**, 25-58 (2002)
[53] http://www.taq.com (data from New York Stock Exchange) and H. Goeppl, Karlsruher Kapitalmarktdatenbank (KKMDB), Institut für Entscheidungstheorie u. Unternehmensforschung, Universität Karlsruhe (TH) (data from Deutsche Börse)

arXiv:cond-mat/0504608v2 [cond-mat.other] 13 May 2006

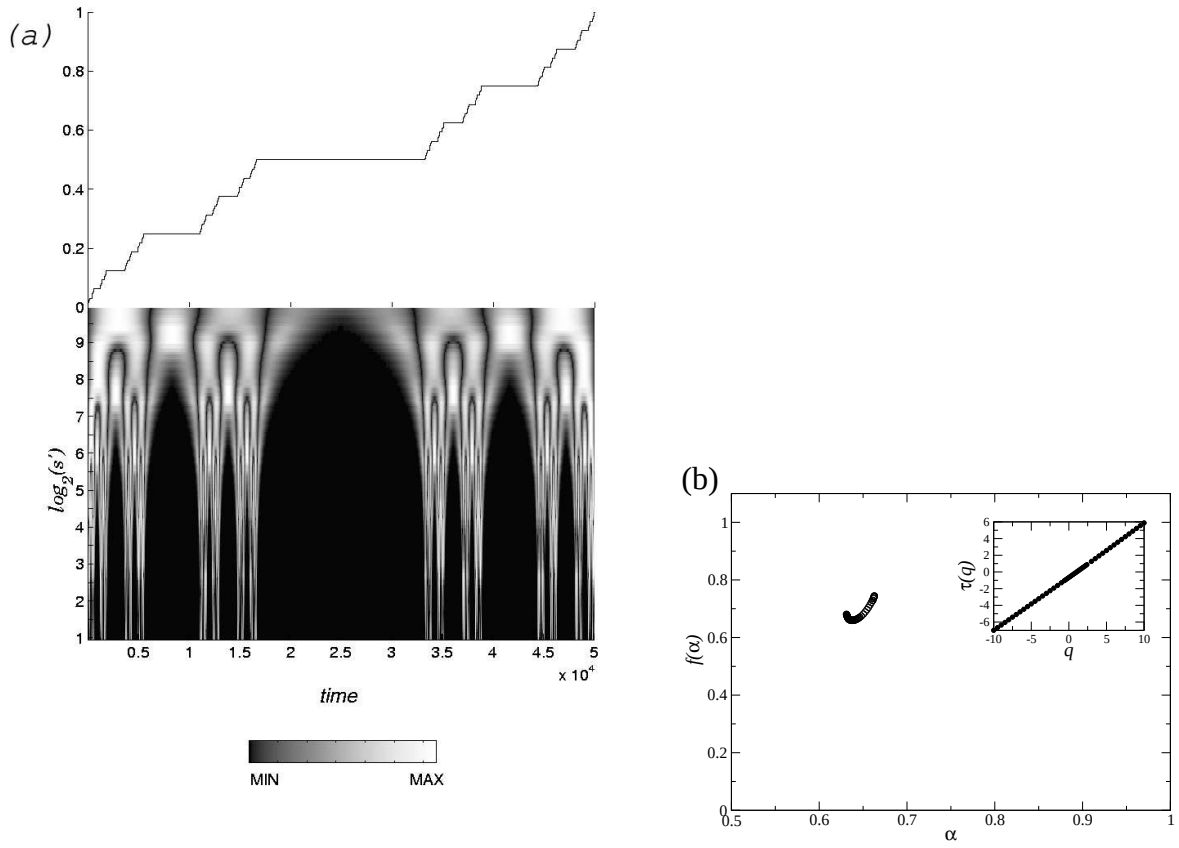


Figure 1: Example of a monofractal function: the devil's staircase obtained by integrating the Cantor measure. (a) Analyzed signal (top) and its wavelet transform T_ψ (bottom) are presented together with (b) the singularity spectrum $f(\alpha)$ (main) and the scaling exponent $\tau(q)$ (inset). The wavelet used in this calculation was $\psi^{(3)}$.

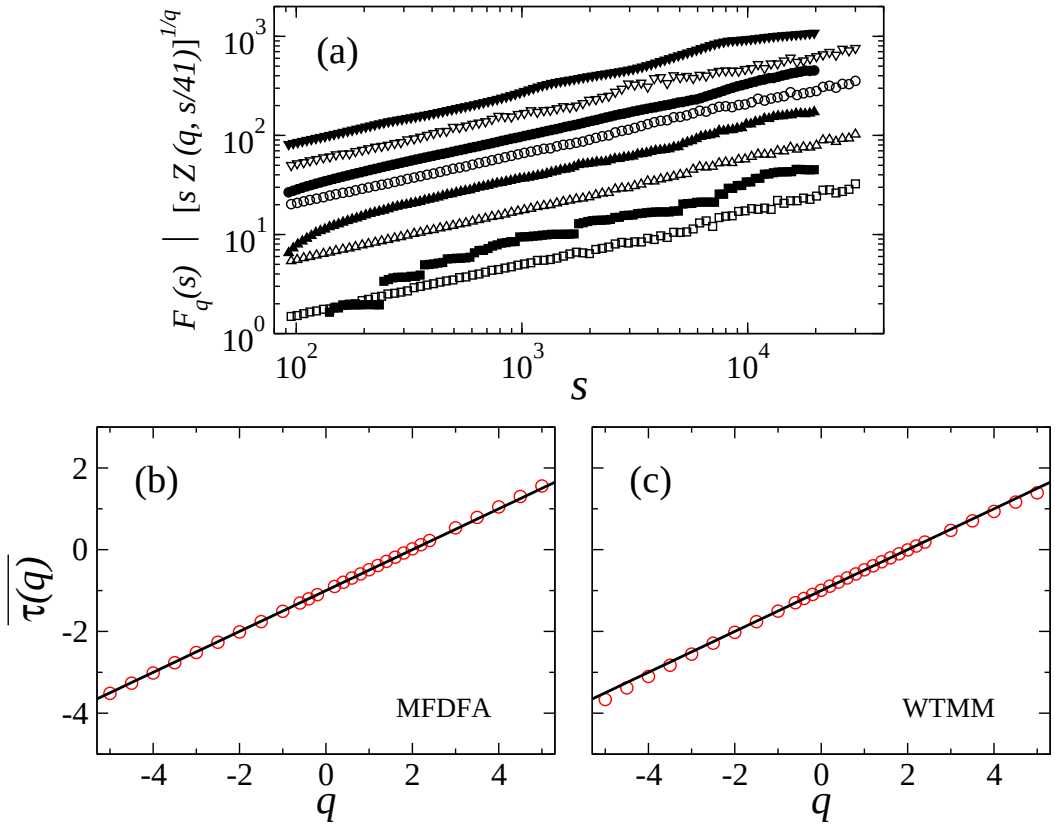


Figure 2: Classical Brownian motion $H = 0.5$: (a) Fluctuation function $F_q(s)$ (open symbols) and rescaled partition function $(sZ(q, s/41))^{1/q}$ (filled symbols) for different values of Rényi parameter: $q = -5$ (squares), $q = -2$ (triangles up), $q = 2$ (circles), and $q = 5$ (triangles down). Note that the plots for different q's were vertically shifted in order to improve readability. Calculations were carried out on time series of length $N = 130,000$ by applying $P^{(2)}$ and $\psi^{(3)}$. Functional dependence of mean scaling exponent $\overline{\tau(q)}$ was derived from $F_q(s)$ in MFDFA (b) and from $Z(q, s')$ in WTMM (c) and compared with its theoretical form (solid line).

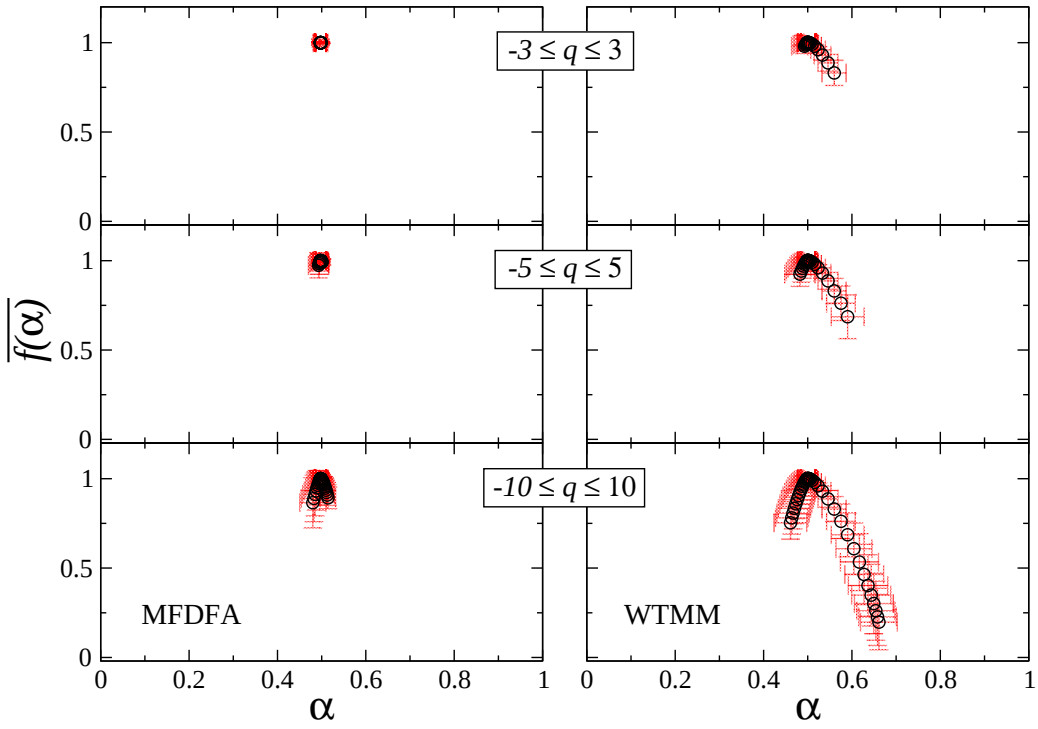


Figure 3: Classical Brownian motion $H = 0.5$: Mean singularity spectra $\overline{f(\alpha)}$ (open circles) obtained by using MFDFA ($P^{(2)}$, left column) and WTMM ($\psi^{(3)}$, right column) procedures for different range of Rényi parameter q: $-3 \leq q \leq 3$ (top), $-5 \leq q \leq 5$ (middle), and $-10 \leq q \leq 10$ (bottom). Time series of length $N = 130,000$ were used; error bars indicate standard deviation of data points calculated from 10 independent realizations of the process.

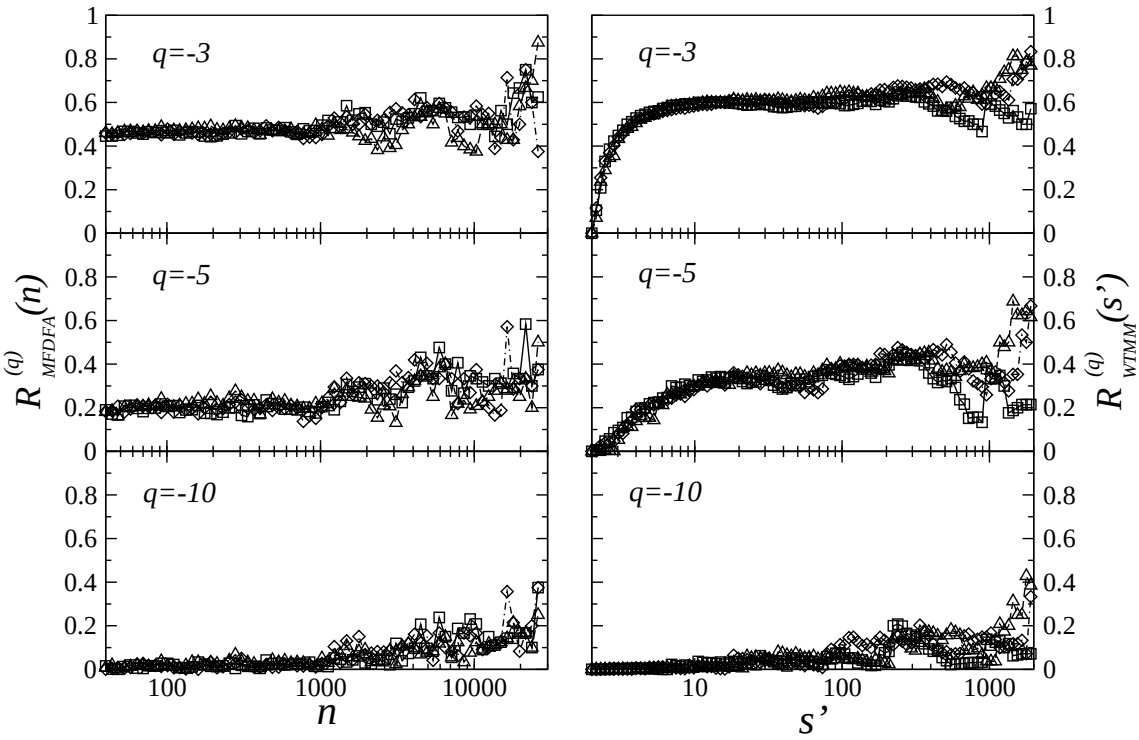


Figure 4: Classical Brownian motion $H = 0.5$: Fraction $R^{(q)}$ of the total number of signal segments (MFDFA) and of the total number of the maxima lines $l \in L(s')$ (WTMM) effectively used in calculation of $F_q(n)$ for MFDFA ($P^{(2)}$, left column) and of $Z(q, s')$ for WTMM ($\psi^{(3)}$, right column). Plots for different negative values of q are shown: $q = -3$ (top), $q = -5$ (middle), and $q = -10$ (bottom), with three different independent process realizations of length $N = 130,000$ (denoted by distinct symbols and lines). Note that for both methods only such ranges of n and s' that were associated with the central stable parts of $R^{(q)}$ were considered in calculation of $\tau(q)$.

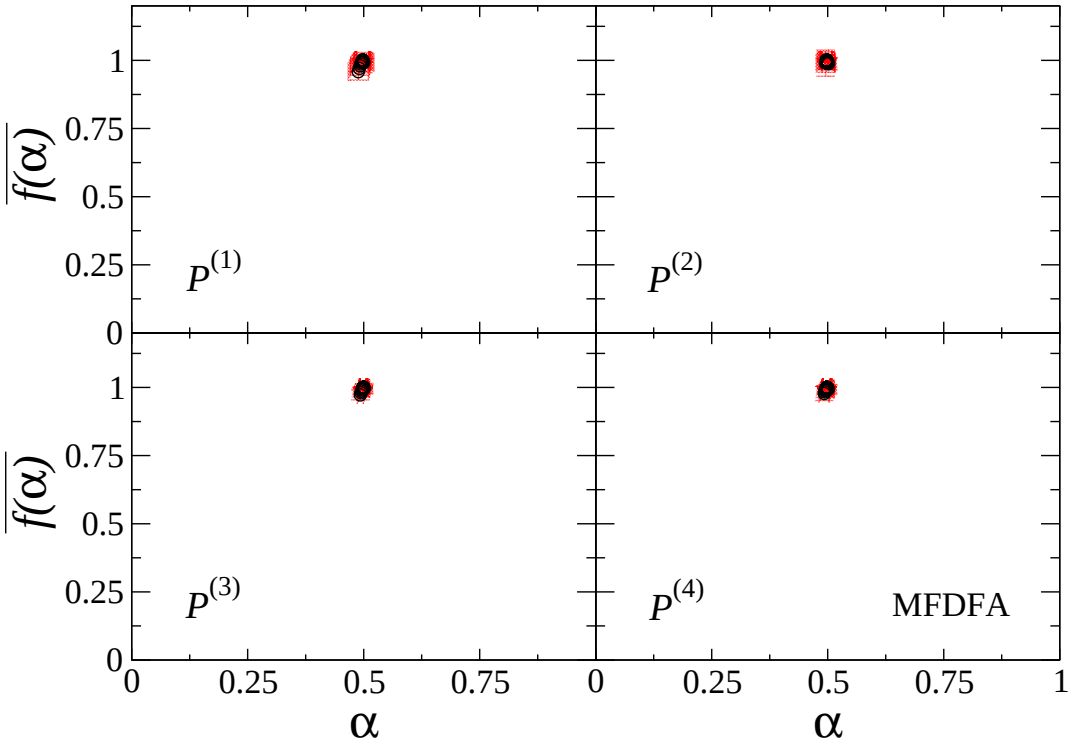


Figure 5: Classical Brownian motion $H = 0.5$: $\overline{f(\alpha)}$ (open circles) for different time series lengths: $N = 15,000$ (top), $N = 65,000$ (middle), and $N = 130,000$ (bottom). Performance of MFDFA ($P^{(2)}$, left column) and WTMM ($\psi^{(3)}$, right column) is compared. Error bars indicate standard deviation of data points calculated from 10 independent realizations of the process.

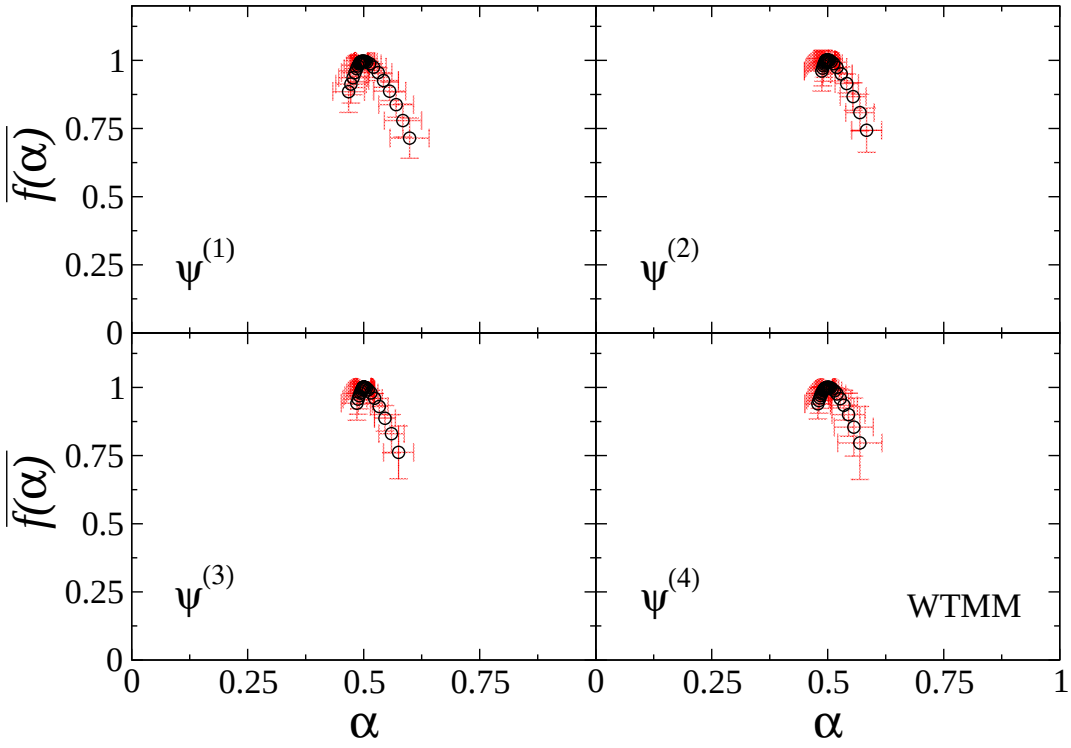


Figure 6: Classical Brownian motion $H = 0.5$: $\overline{f(\alpha)}$ (open circles) obtained with MFDFA for different polynomials: from $P^{(1)}$ (top left) to $P^{(4)}$ (bottom right). Time series of length $N = 130,000$ were used; error bars indicate standard deviation of data points calculated from 10 independent realizations of the process.

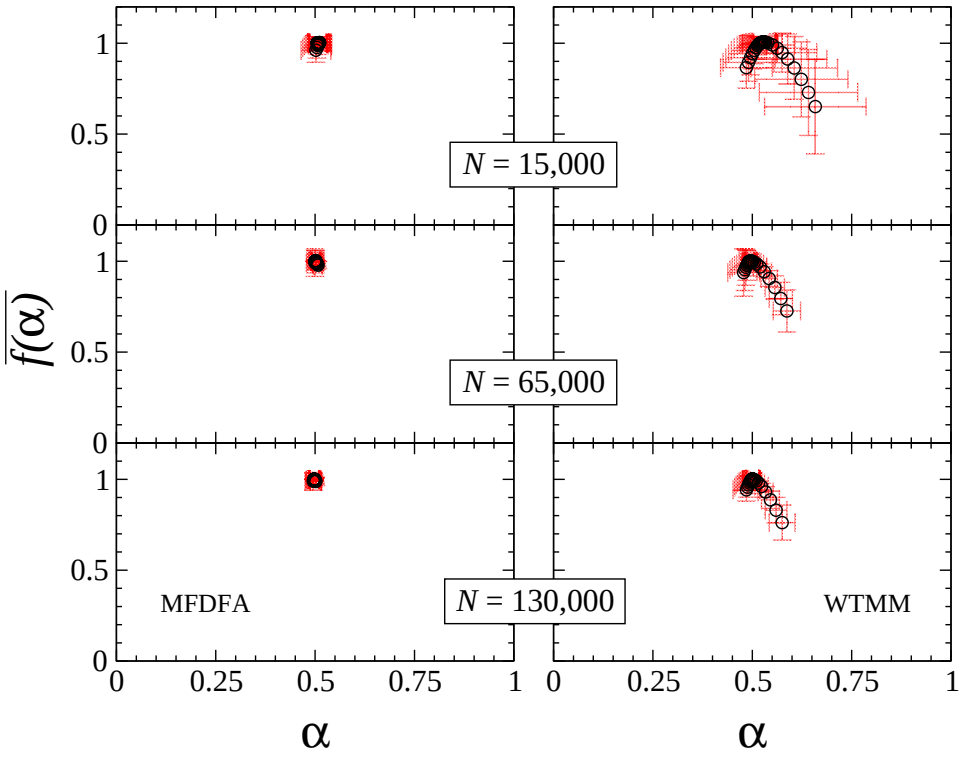


Figure 7: Classical Brownian motion $H = 0.5$: $\overline{f(\alpha)}$ (open circles) obtained with WTMM for different wavelets: from $\psi^{(1)}$ (top left) to $\psi^{(4)}$ (bottom right). Time series of length $N = 130,000$ were used; error bars indicate standard deviation of data points calculated from 10 independent realizations of the process.

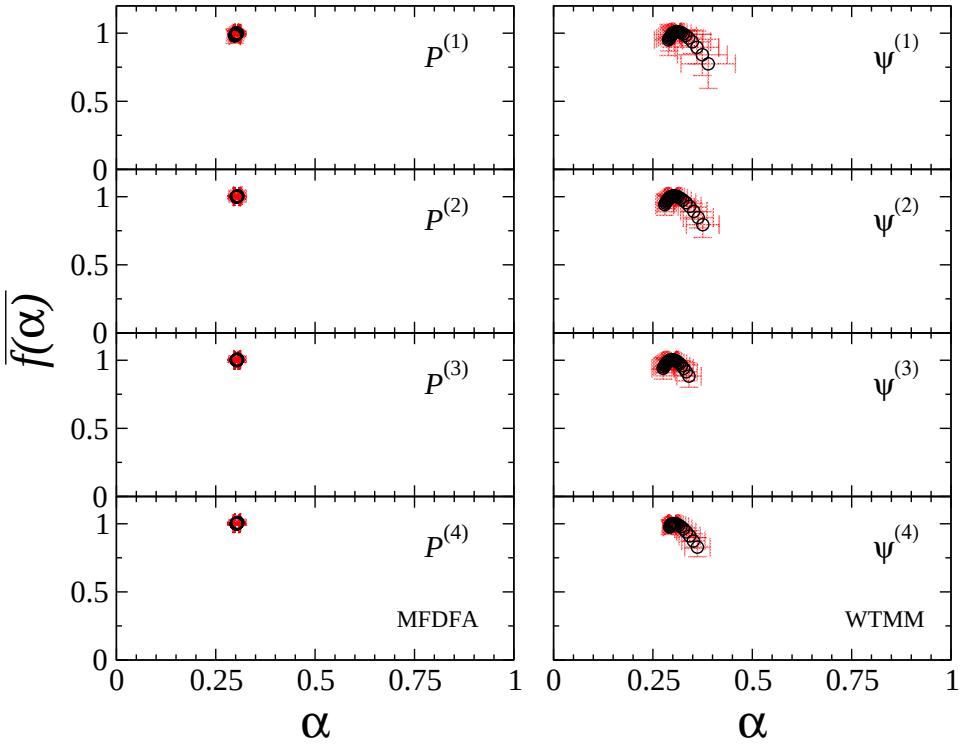


Figure 8: Antipersistent fractional Brownian motion $H = 0.3$: $\overline{f(\alpha)}$ (open circles) for different polynomials $P^{(l)}$ of MFDFA (left column) and for different Gaussian derivatives $\psi^{(m)}$ of WTMM (right column). Time series of length $N = 130,000$ were used; error bars indicate standard deviation of data points calculated from 10 independent realizations of the process.

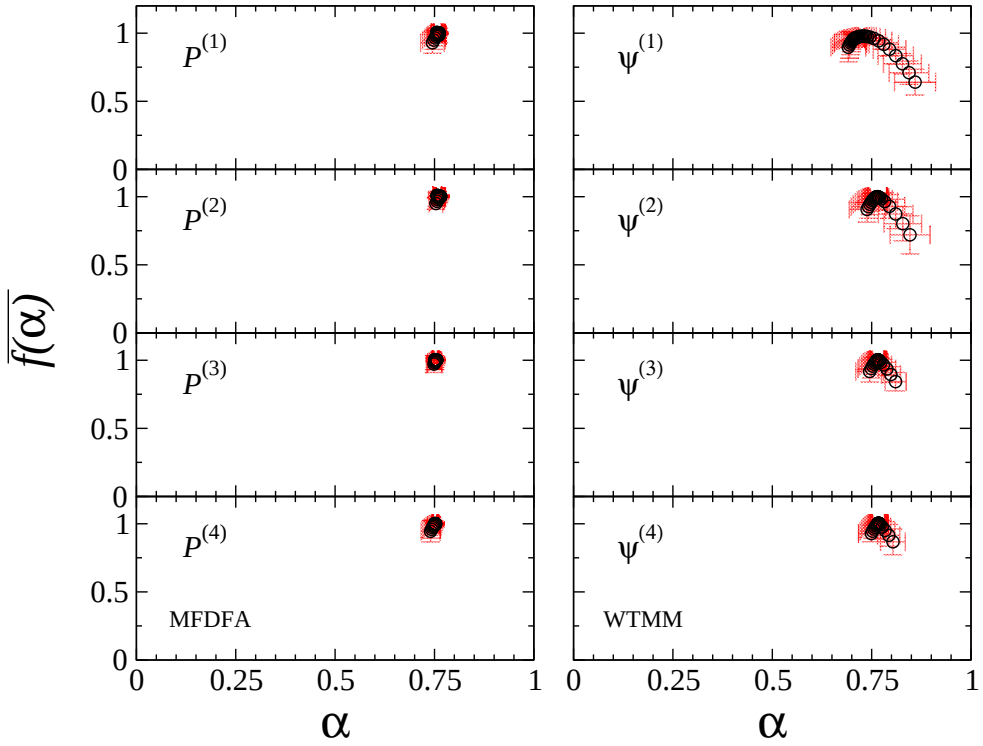


Figure 9: Persistent fractional Brownian motion $H = 0.75$: $\overline{f(\alpha)}$ (open circles) for different polynomials $P^{(l)}$ of MFDFA (left column) and for different Gaussian derivatives $\psi^{(m)}$ of WTMM (right column). Time series of length $N = 130,000$ were used; error bars indicate standard deviation of data points calculated from 10 independent realizations of the process.

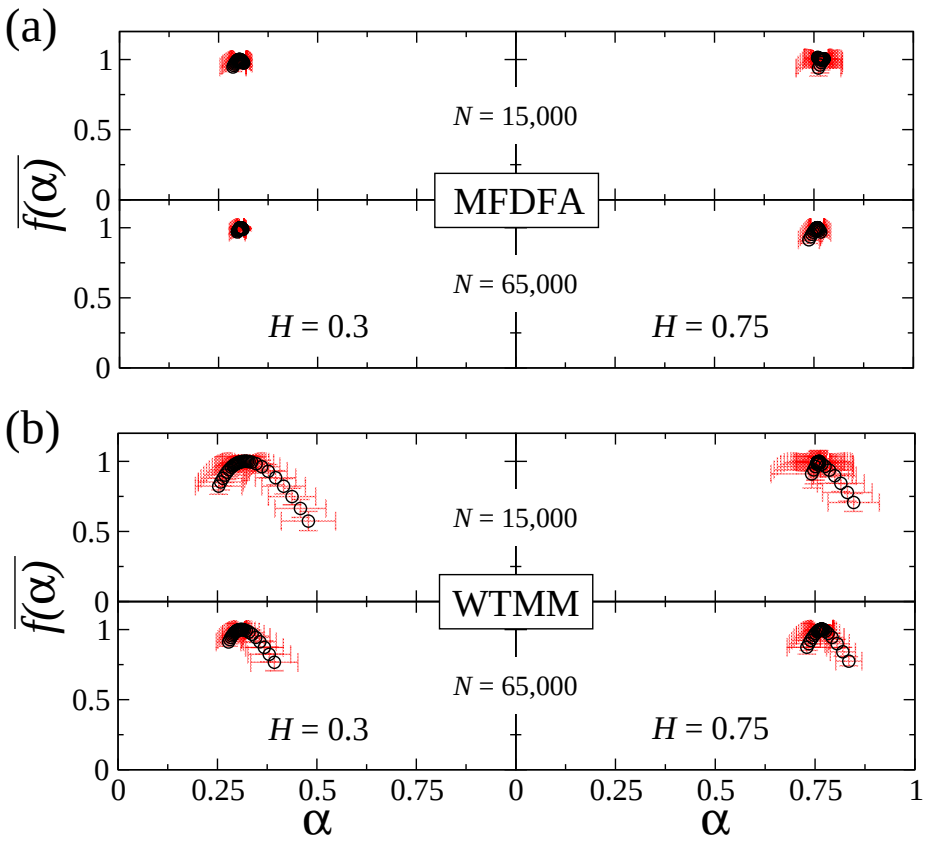


Figure 10: Fractional Brownian motion: (a) MFDFA with $P^{(2)}$ and (b) WTMM with $\psi^{(3)}$: Mean singularity spectra (open circles) for different time series lengths: $N = 15,000$ (top) and $N = 65,000$ (bottom) for the fractional Brownian motion in its antipersistent ($H = 0.3$, left) and persistent ($H = 0.75$, right) variants. Error bars indicate standard deviation of data points calculated from 10 independent realizations of each process. Plots should be compared with te respective panels of Figures 8 and 9, where signals of $N = 130,000$ were used.

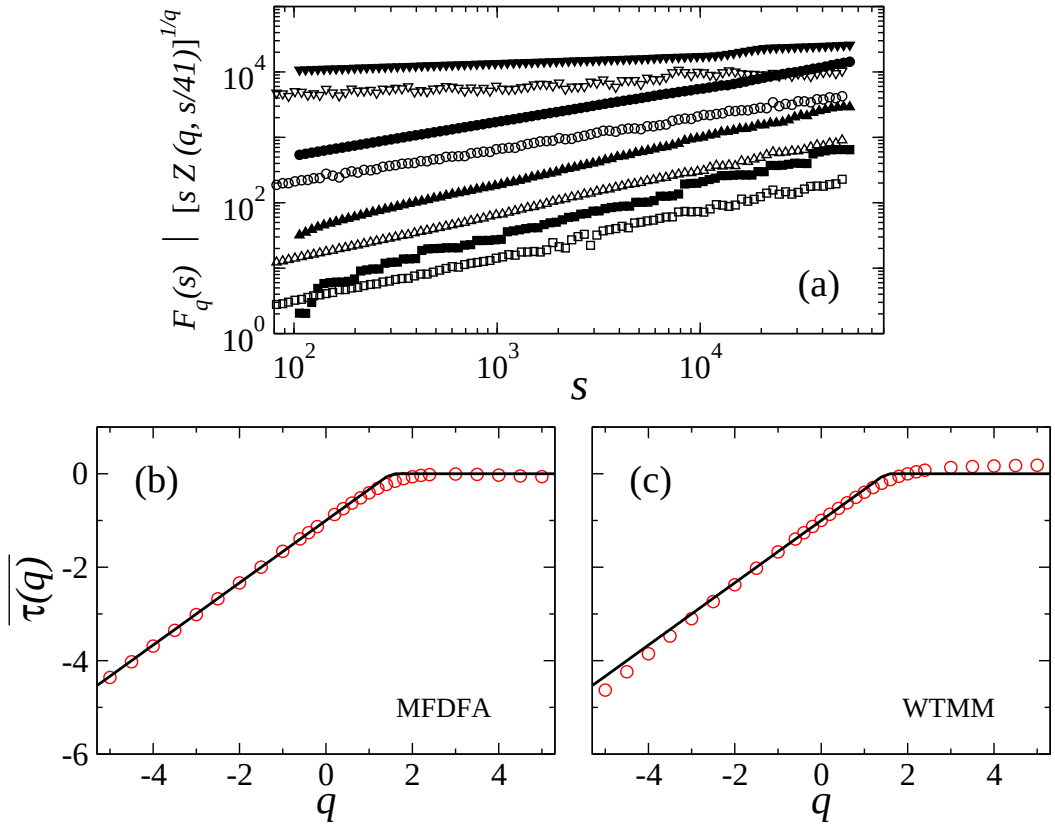


Figure 11: Lévy process $\alpha_L = 1.5$: (a) Fluctuation function $F_q(s)$ (open symbols) and rescaled partition function $(sZ(q, s/41))^{1/q}$ (filled symbols) for different values of Rényi parameter $q = -5$ (squares), $q = -2$ (triangles up), $q = 2$ (circles), and $q = 5$ (triangles down). Calculations were carried out on time series of length $N = 250,000$ by applying $P^{(2)}$ and $\psi^{(3)}$. Functional dependence of mean scaling exponent $\overline{\tau(q)}$ was derived from $F_q(s)$ in MFDFA (b) and from $Z(q, s')$ in WTMM (c) and compared with its theoretical form (solid line).

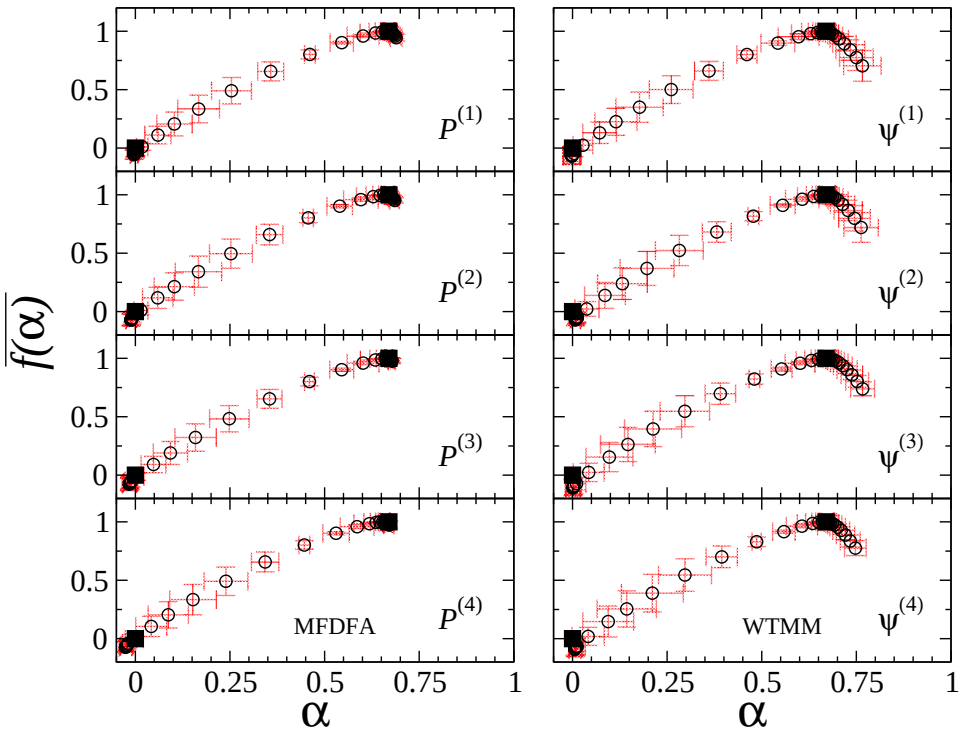


Figure 12: Lévy process $\alpha_L = 1.5$: $\overline{f(\alpha)}$ (open circles) obtained with MFDFA procedure (left column) for different polynomial orders: from $P^{(1)}$ (top) to $P^{(4)}$ (bottom) and with WTMM procedure (right column) for different wavelets: from $\psi^{(1)}$ (top) to $\psi^{(4)}$ (bottom) compared with the corresponding exact theoretical values of $f(\alpha)$ (filled squares). Time series of length $N = 250,000$ were used; error bars indicate standard deviation of data points calculated from 10 independent realizations of the process.

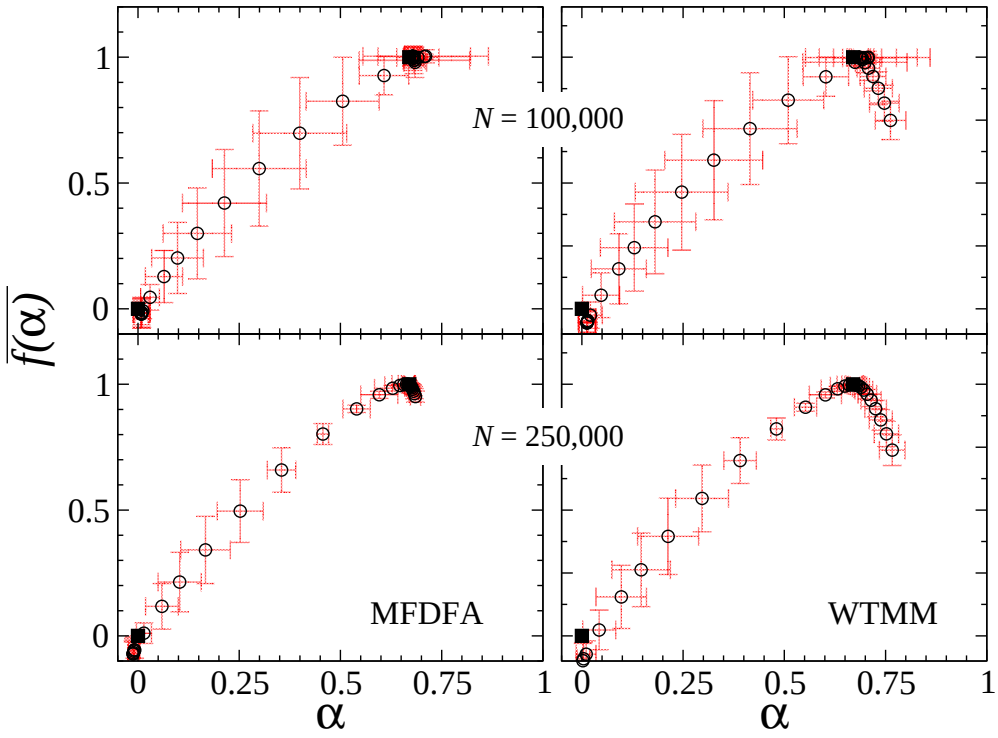


Figure 13: Lévy process $\alpha_L = 1.5$: $\overline{f(\alpha)}$ (open circles) for different time series lengths: $N = 100,000$ (top) and $N = 250,000$ (bottom) together with the corresponding theoretical values of $f(\alpha)$ (filled squares). Performance of MFDFA ($P^{(2)}$, left column) and WTMM ($\psi^{(3)}$, right column) is compared. Error bars indicate standard deviation of data points calculated from 10 independent realizations of the process.

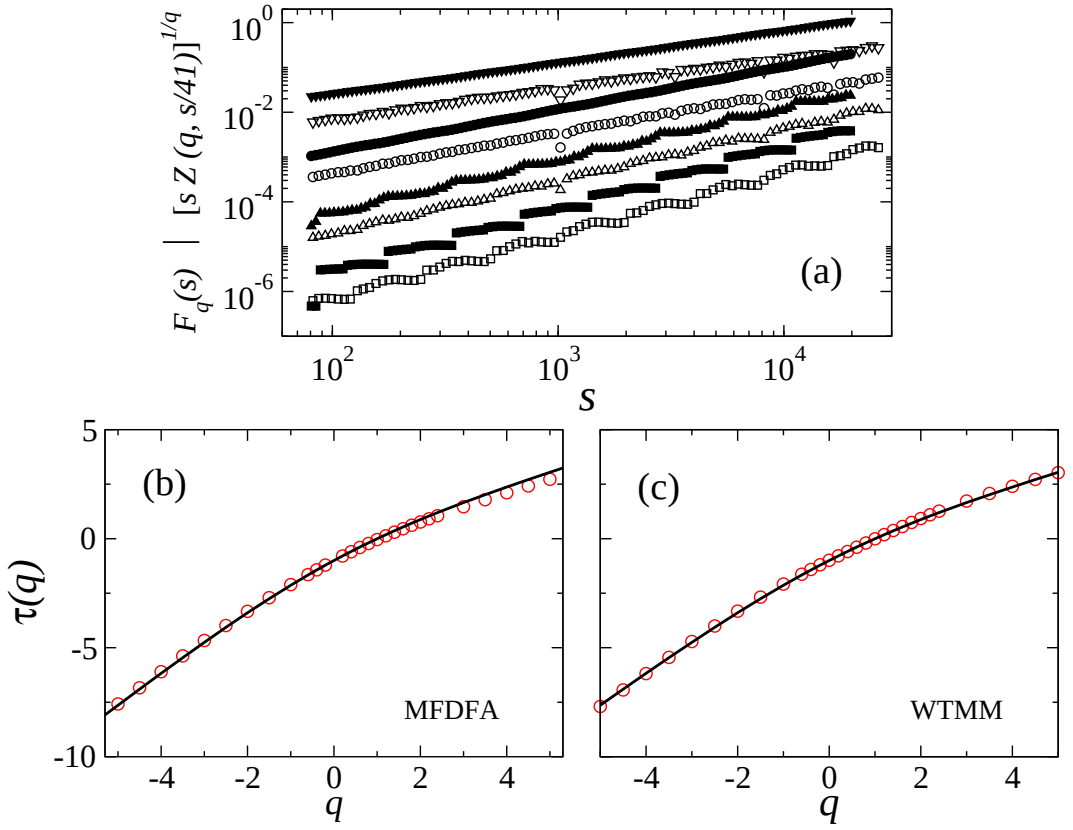


Figure 14: Deterministic binomial cascade $a = 0.65$: (a) Examples of fluctuation function $F_q(s)$ and rescaled partition function $(sZ(q, s/41))^{1/q}$ for different values of Rényi parameter: $q = -5$ (squares), $q = -2$ (triangles up), $q = 2$ (circles), and $q = 5$ (triangles down). (b) and (c) Scaling exponents $\tau(q)$ for MFDFA ($P^{(2)}$) and for WTMM ($\psi^{(3)}$) are presented together with their theoretical behaviour (solid line). Cascade was generated in $k = 17$ stages and its length was equal to $N = 131,072$ points.

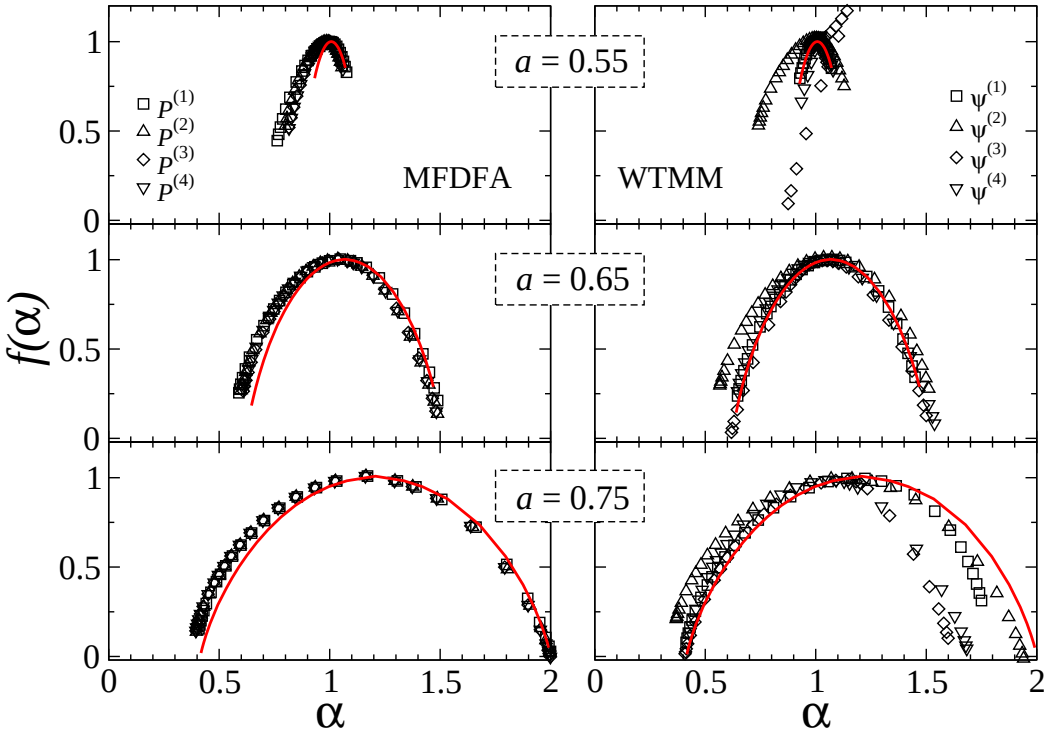


Figure 15: Deterministic binomial cascade: Singularity spectra (open circles) for different mass allocations between subintervals: $a = 0.55$ (top), $a = 0.65$ (middle), and $a = 0.75$ (bottom). Left column: results from MFDFA with different polynomials: $P^{(1)}$ (squares), $P^{(2)}$ (triangles up), $P^{(3)}$ (diamonds), and $P^{(4)}$ (triangles down). Right column: results from WTMM with different wavelets: $\psi^{(1)}$ (circles), $\psi^{(2)}$ (triangles up), $\psi^{(3)}$ (diamonds), and $\psi^{(4)}$ (triangles down). Theoretical $f(\alpha)$ spectra are denoted by solid lines. Cascade was generated in $k = 17$ stages and its length was equal to $N = 131,072$ points.

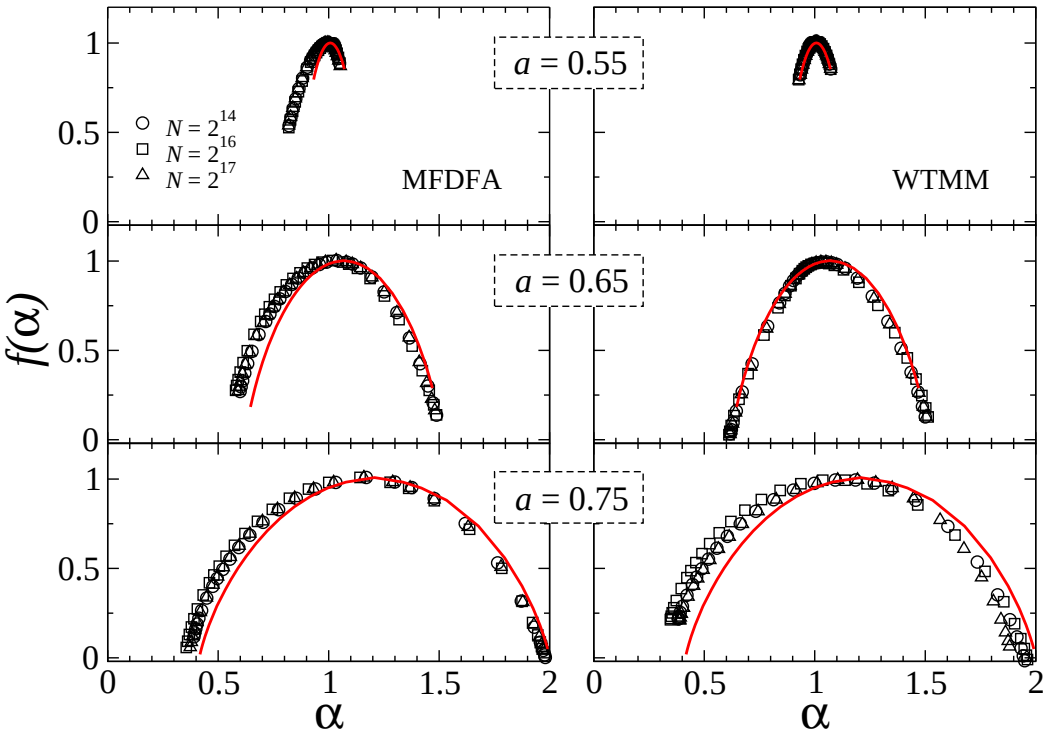


Figure 16: Deterministic binomial cascade with $a = 0.55$ (top), $a = 0.65$ (middle), and $a = 0.75$ (bottom): Singularity spectra (open circles) for different cascade stages: $k = 14$ ($N = 16,384$, circles), $k = 16$ ($N = 65,536$, squares), and $k = 17$ ($N = 131,072$, triangles) together with the corresponding theoretical spectrum (solid line). Left column: results from MFDFA with $P^{(2)}$. Right column: results from WTMM; for each value of parameter a a wavelet with the best performance (see Figure 15) is used: $\psi^{(1)}$ (top), $\psi^{(3)}$ (middle), and $\psi^{(2)}$ (bottom).

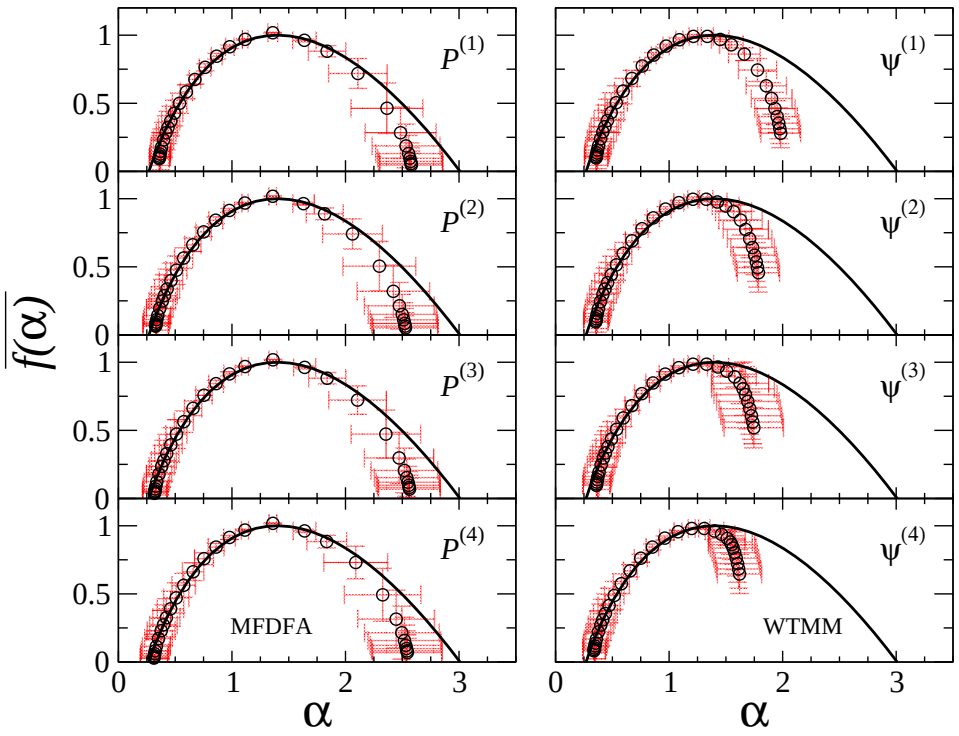


Figure 17: Log-Poisson binomial cascade with $\gamma = 1.4$: Mean singularity spectra $\overline{f(\alpha)}$ (open circles) obtained with MFDFA (left column) for different polynomials: from $P^{(1)}$ (top) to $P^{(4)}$ (bottom) and with WTMM (right column) for different wavelets: from $\psi^{(1)}$ (top) to $\psi^{(4)}$ (bottom), compared with the corresponding theoretical spectrum (solid lines). Cascade was generated in $k = 17$ stages ($N = 131,072$). Error bars indicate standard deviation of data points calculated from 10 independent realizations of the process.

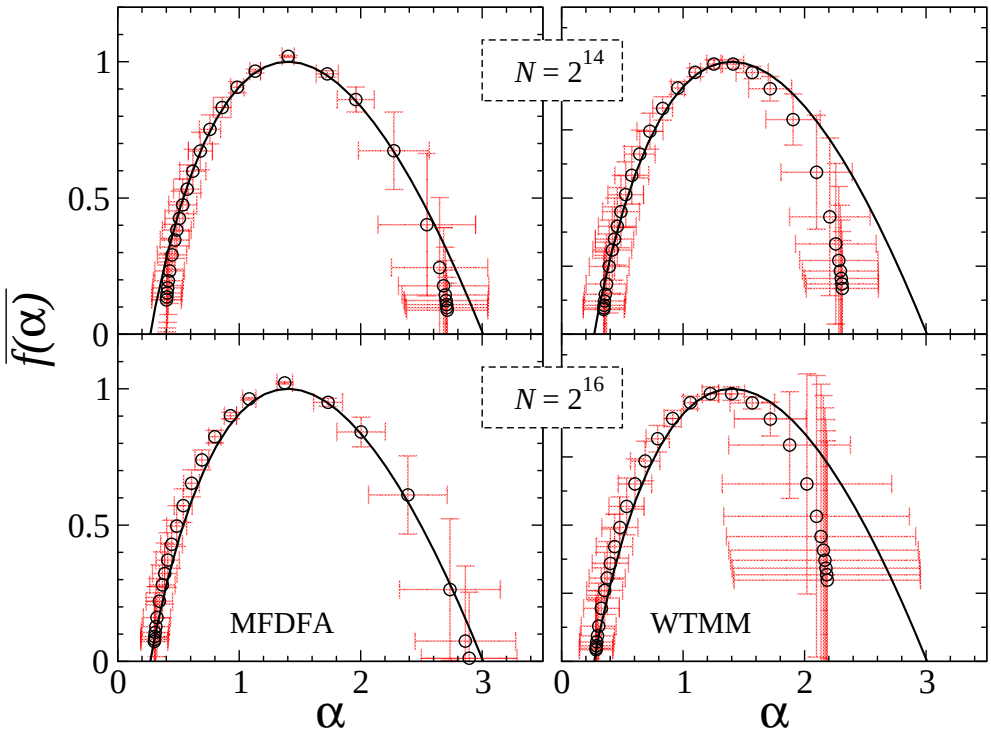


Figure 18: Log-Poisson binomial cascade with $\gamma = 1.4$: $\overline{f(\alpha)}$ (open circles) for different cascade stages: $k = 14$ ($N = 16,384$, top), and $k = 16$ ($N = 65,536$, bottom) together with theoretical spectrum (solid lines). Performance of MFDFA ($P^{(2)}$, left column) and WTMM ($\psi^{(3)}$, right column) is compared. Error bars indicate standard deviation of data points calculated from 10 independent realizations of the process. Plots should be compared with the corresponding panels of Figure 17, where the results for signals of $k = 17$ ($N = 131,072$) are shown.

arXiv:cond-mat/0504608v2 [cond-mat.other] 13 May 2006

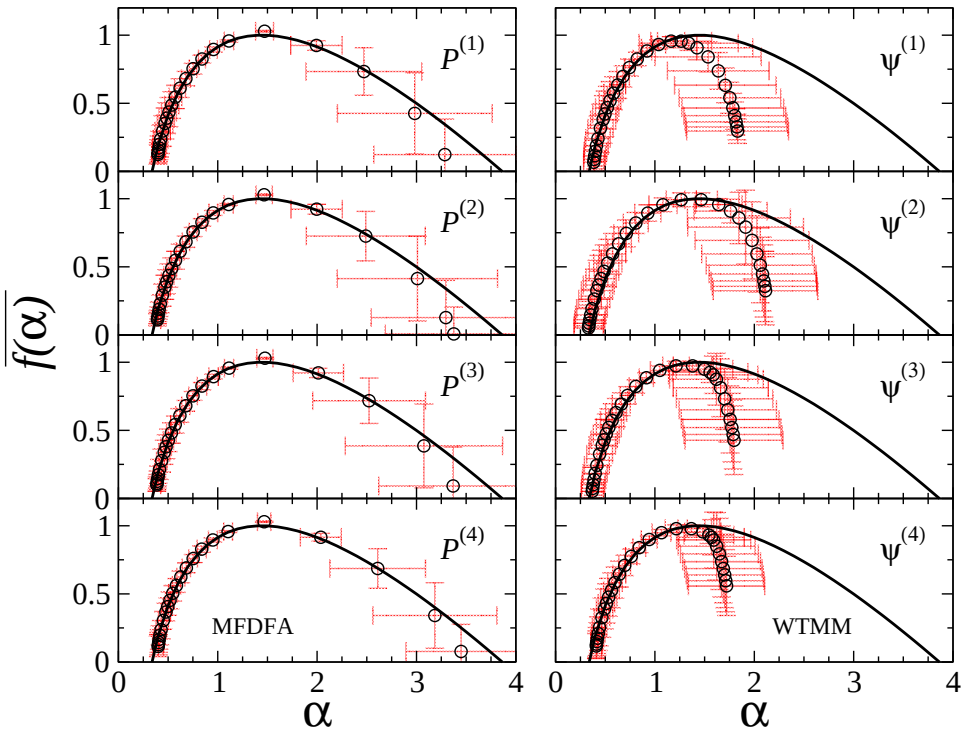


Figure 19: Log-gamma binomial cascade with $\gamma = 1$, $\beta = \ln 2$: $\overline{f(\alpha)}$ (open circles) obtained with MFDFA (left column) for different polynomials: from $P^{(1)}$ (top) to $P^{(4)}$ (bottom) and with WTMM (right column) for different wavelets: from $\psi^{(1)}$ (top) to $\psi^{(4)}$ (bottom), compared with theoretical spectra (solid lines). Cascade was generated in $k = 17$ stages ($N = 131,072$). Error bars indicate standard deviation of data points calculated from 10 independent realizations of the process.

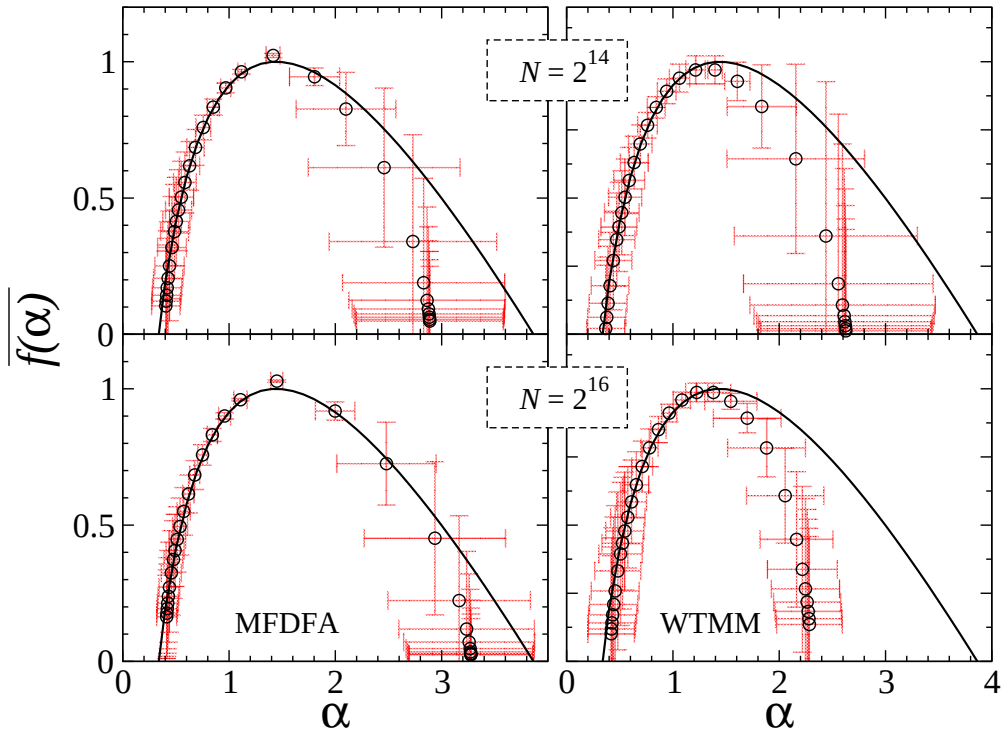


Figure 20: Log-gamma binomial cascade with $\gamma = 1, \beta = \ln 2$: $\overline{f(\alpha)}$ (open circles) for different cascade stages: $k = 14$ ($N = 16,384$, top) and $k = 16$ ($N = 65,536$, bottom) together with theoretical $f(\alpha)$ (solid lines). Performance of MFDFA ($P^{(2)}$, left column) and WTMM ($\psi^{(3)}$, right column) is compared. Error bars indicate standard deviation of data points calculated from 10 independent realizations of the process. Plots should be compared with the corresponding panels of Figure 19, where the results for signals of $k = 17$ ($N = 131,072$) are shown.

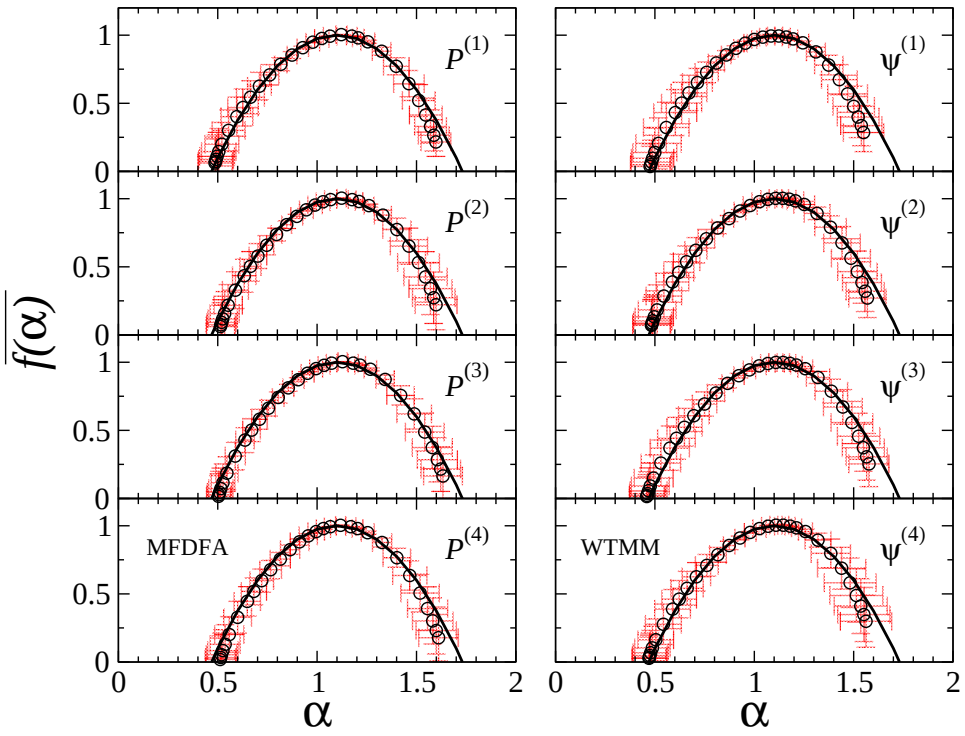


Figure 21: Log-normal binomial cascade with $\lambda = 1.1$: $\overline{f(\alpha)}$ (open circles) obtained with MFDFA (left column) for different polynomials: from $P^{(1)}$ (top) to $P^{(4)}$ (bottom) and with WTMM (right column) for different wavelets: from $\psi^{(1)}$ (top) to $\psi^{(4)}$ (bottom) compared with the theoretical spectra (solid lines). Cascade was generated in $k = 17$ stages ($N = 131,072$). Error bars indicate standard deviation of data points calculated from 10 independent realizations of the process.

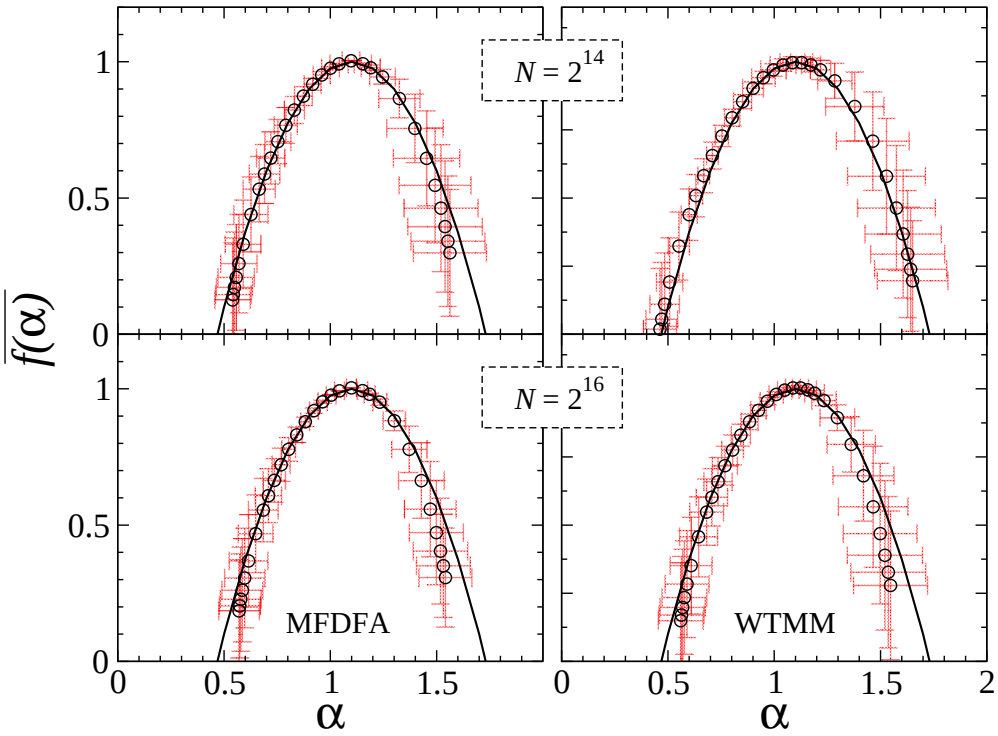


Figure 22: Log-normal binomial cascade with $\lambda = 1.1$: $\overline{f(\alpha)}$ (open circles) for different cascade stages: $k = 14$ ($N = 16,384$, top), and $k = 16$ ($N = 65,536$, bottom) together with theoretical $f(\alpha)$ (solid lines). Performance of MFDFA ($P^{(2)}$, left column) and WTMM ($\psi^{(3)}$, right column) is compared. Error bars indicate standard deviation of data points calculated from 10 independent realizations of the process. Plots should be compared with the corresponding panels of Figure 19, where the results for signals of $k = 17$ ($N = 131,072$) are shown.

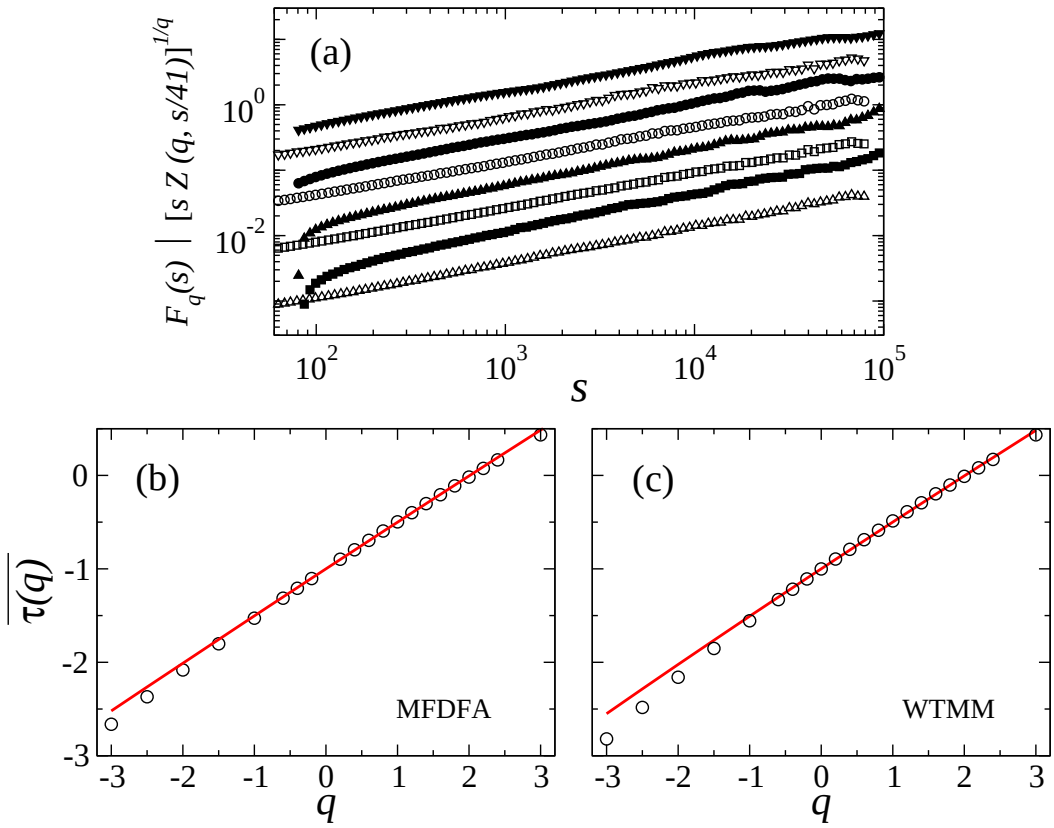


Figure 23: (a) Transaction-to-transaction logarithmic price increments of exemplary stock traded on Deutsche Börse: Volkswagen (VOW): Examples of fluctuation function $F_q(s)$ and rescaled partition function $(sZ(q, s/41))^{1/q}$ for different values of Rényi parameter: $q = -5$ (squares), $q = -2$ (triangles up), $q = 2$ (circles), and $q = 5$ (triangles down). (b) and (c) Mean scaling exponent $\overline{\tau(q)}$ for MFDFA ($P^{(2)}$) and for WTMM ($\psi^{(3)}$) calculated from stocks corresponding to 30 companies of DAX (empty circles). Straight lines in bottom panels denote a monofractal, linearly uncorrelated reference signal.

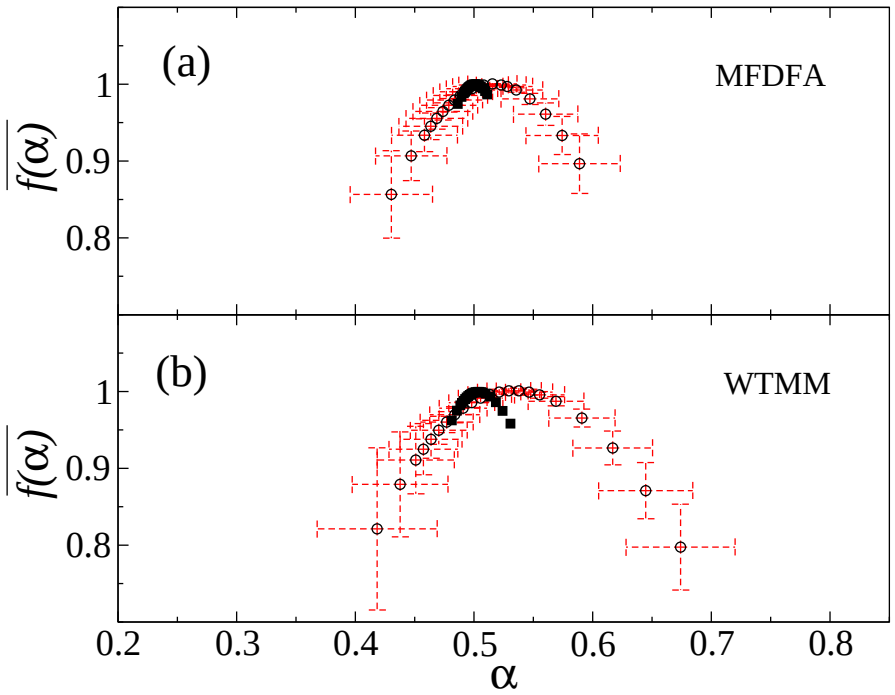


Figure 24: Mean $f(\alpha)$ spectra obtained by MFDFA (a) and by WTMM (b) for 30 stocks corresponding to DAX companies (empty circles) together with their randomly reshuffled counterparts (full squares). Error bars for the original data denote standard deviation of data points calculated from 30 stocks.

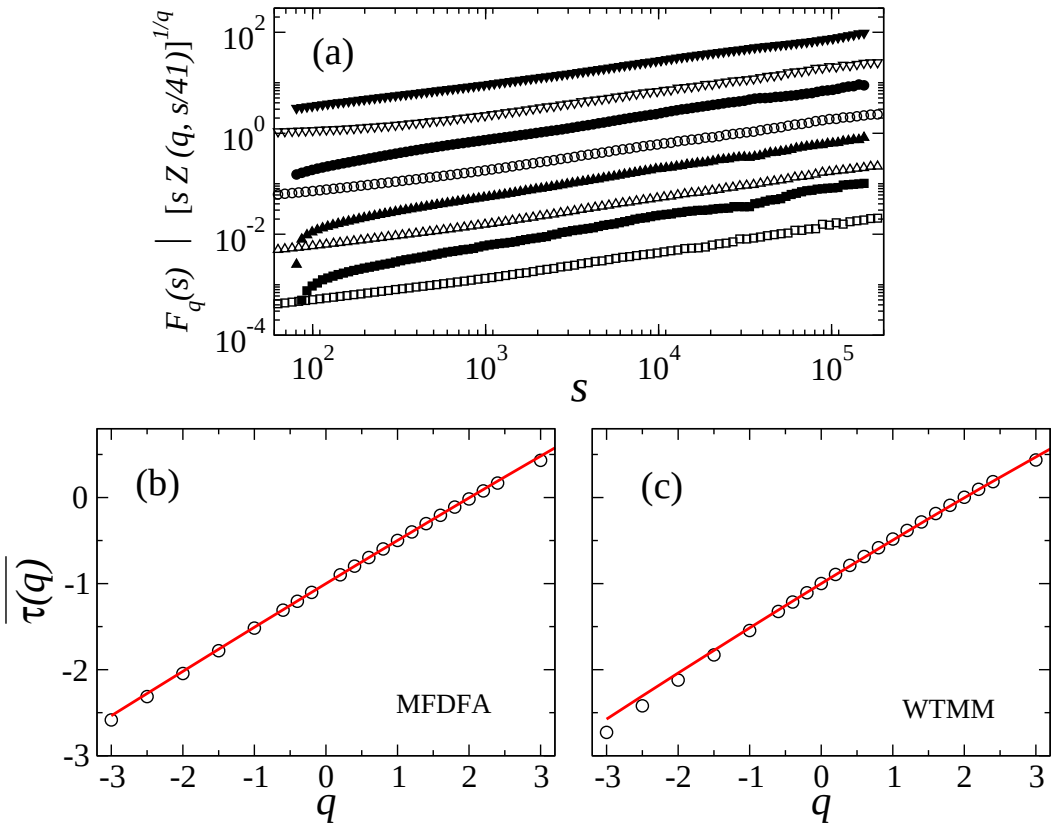


Figure 25: (a) Transaction-to-transaction logarithmic price increments of exemplary DJI stock: IBM Corp.: Examples of fluctuation function $F_q(s)$ and rescaled partition function $(sZ(q, s/41))^{1/q}$ for different values of Rényi parameter: $q = -5$ (squares), $q = -2$ (triangles up), $q = 2$ (circles), and $q = 5$ (triangles down). (b) and (c) Mean scaling exponent $\overline{\tau(q)}$ for MFDFA ($P^{(2)}$) and for WTMM ($\psi^{(3)}$) calculated from stocks corresponding to 30 DJI companies (empty circles). Straight lines in bottom panels denote a monofractal, linearly uncorrelated reference signal.

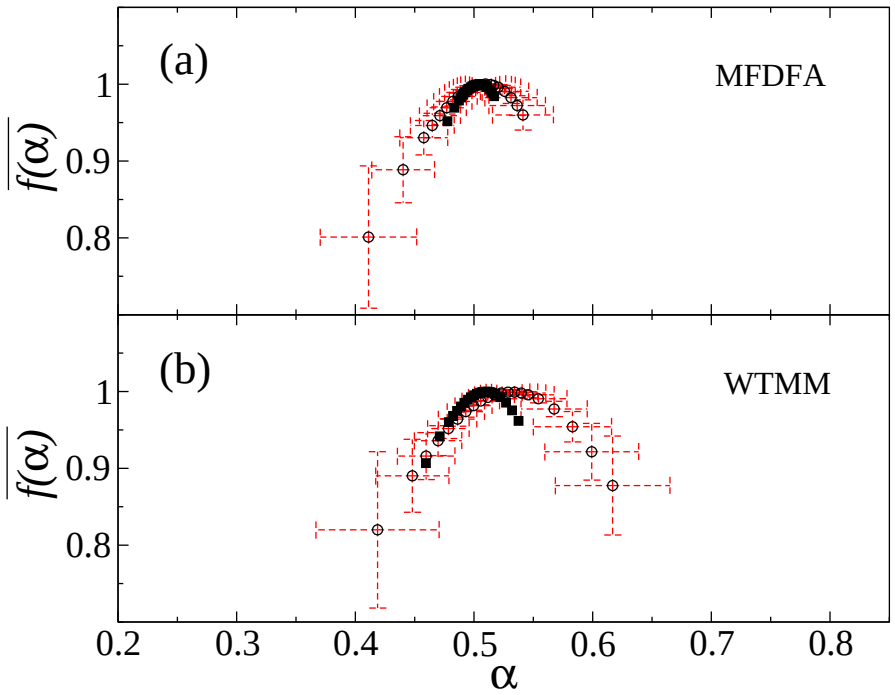


Figure 26: $\overline{f(\alpha)}$ obtained by MFDFA (a) and by WTMM (b) for 30 stocks corresponding to DJI companies (empty circles) together with their randomly reshuffled counterparts (full squares). Error bars for the original data denote standard deviation of data points calculated from 30 stocks.